HHS Public Access

Author manuscript

Cell Rep. Author manuscript; available in PMC 2019 May 10.

Published in final edited form as:

Cell Rep. 2019 March 05; 26(10): 2818–2832.e8. doi:10.1016/j.celrep.2019.02.011.

Functional Access to Neuron Subclasses in Rodent and Primate Forebrain

Preeti Mehta[1,4], **Lauren Kreeger**[1,4], **Dennis C. Wylie**[7], **Jagruti J. Pattadkal**[1,2,4], **Tara Lusignan**[1,4], **Matthew J. Davis**[1,4], **Gergely F. Turi**[3,6], **Wen-Ke Li**[3,6], **Matthew P. Whitmire**[2,4,5], **Yuzhi Chen**[2,4,5], **Bridget L. Kajs**[1,4], **Eyal Seidemann**[2,4,5], **Nicholas J. Priebe**[1,2,4], **Attila Losonczy**[3,6], and **Boris V. Zemelman**[1,4,8,*]

[1]Center for Learning and Memory, University of Texas, Austin, TX 78712, USA

[2]Center for Perceptual Systems, University of Texas, Austin, TX 78712, USA

[3]Kavli Institute for Brain Science, Columbia University, New York, NY 10027, USA

[4]Department of Neuroscience, University of Texas, Austin, TX 78712, USA

[5]Department of Psychology, University of Texas, Austin, TX 78712, USA

[6]Department of Neuroscience, Columbia University, New York, NY 10027, USA

[7]Center for Computational Biology and Bioinformatics, University of Texas, Austin, TX 78712, USA

[8]Lead Contact

SUMMARY

Viral vectors enable foreign proteins to be expressed in brains of non-genetic species, including non-human primates. However, viruses targeting specific neuron classes have proved elusive. Here we describe viral promoters and strategies for accessing GABAergic interneurons and their molecularly defined subsets in the rodent and primate. Using a set intersection approach, which relies on two co-active promoters, we can restrict heterologous protein expression to cortical and hippocampal somatostatin-positive and parvalbumin-positive interneurons. With an orthogonal set difference method, we can enrich for subclasses of neuropeptide-Y-positive GABAergic interneurons by effectively subtracting the expression pattern of one promoter from that of another.

*Correspondence: zemelmanb@mail.clm.utexas.edu.

AUTHOR CONTRIBUTIONS

Conceptualization, B.V.Z.; Methodology, A.L., P.M., N.J.P., E.S., and B.V.Z.; Software, D.C.W. and A.L.; Validation, P.M., L.K., and T.L.; Investigation, M.J.D., G.F.T., W.-K.L., A.L., J.J.P., Y.C., M.P.W., N.J.P., and E.S.; Resources, P.M., D.C.W., B.L.K., and B.V.Z.; Writing – Original Draft, P.M. and B.V.Z.; Writing – Review & Editing, A.L., P.M., N.J.P., E.S., and B.V.Z.; Project Administration, A.L., N.J.P., E.S., and B.V.Z.; Funding Acquisition, A.L., N.J.P., E.S., and B.V.Z.

SUPPLEMENTAL INFORMATION

Supplemental Information can be found with this article online at https://doi.org/10.1016/j.celrep.2019.02.011.

DECLARATION OF INTERESTS

The authors declare no competing interests. The University of Texas has filed a provisional patent application covering the methods and preparations described in this article.

SUPPORTING CITATIONS

The following reference appears in the Supplemental Information: Hu et al. (2014).

These methods harness the complexity of gene expression patterns in the brain and significantly expand the number of genetically tractable neuron classes across mammals.

Graphical Abstract

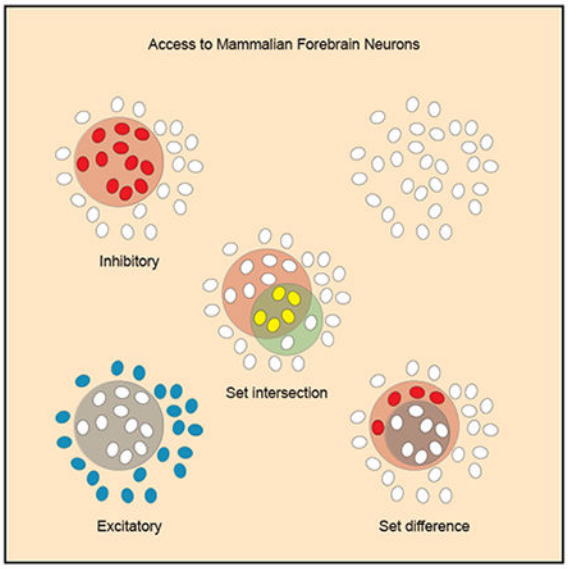

In Brief

Mehta et al. describe methods for accessing inhibitory neuron subclasses in the mammalian forebrain.

INTRODUCTION

Functional dissection of mammalian neuronal circuits is predicated on an ability to accurately target constituent cell classes. Transgenic approaches in rodents, particularly in mice, have proved useful, offering a precise and predictable way to access genetically defined cell populations for subsequent manipulations (He et al., 2016; Murray et al., 2012; Taniguchi et al., 2011). However, rodent line derivation represents a trade-off between reliability and convenience: costly and time-consuming techniques designed to produce genetic animal models are poor vehicles for expressing engineered proteins that can become obsolete during the animal's lifespan. There is also the pressing need to target genetically and molecularly specified neuronal populations in the primate, an important animal model for human perception, cognition, and action, which is less amenable to genomic manipulations. Viral vectors, simpler to generate and easy to deploy, represent an attractive alternative to transgenics and are used widely to express heterologous proteins (Betley and Sternson, 2011). These vectors, such as recombinant adeno-associated viruses (rAAVs), are non-pathogenic, infect neurons of multiple species, and offer the added benefits of spatial and temporal control over transgene expression (Samulski et al., 1989; Tenenbaum et al., 2004).

One shortcoming of viral vectors, however, has been their limited cell type specificity in the brain: with the exceptions of specialized cell classes, such as dopaminergic, amacrine, and Purkinje neurons (Borghuis et al., 2011; El-Shamayleh et al., 2017; Stauffer et al., 2016) and pan-excitatory neurons (Dittgen et al., 2004; Han et al., 2009; Seidemann et al., 2016), restricting heterologous protein expression to subsets of excitatory and inhibitory neurons using viruses has proved difficult (Nathanson et al., 2009b; but see Dimidschstein et al., 2016; Lee et al., 2014). This is because the requisite promoter elements have not been described, and viral payload is limited, foreclosing the use of proximal chromosomal segments that represents a workaround prevalent in mouse transgenics.

We were particularly interested in targeting GABAergic interneurons, which account for fewer than a quarter of neurons in the mammalian cortex (Meyer et al., 2011) but play key roles in cortical computations (Allen et al., 2011; Caputi et al., 2013; Fuchs et al., 2007). To identify promoters active across GABAergic neurons, we focused on the conserved enhancer-like sequences interspersed among *Dlx* homeobox transcription factor genes that are expressed in interneurons during embryonic and postnatal development (Cobos et al., 2005, 2007; Long et al., 2009; Stühmer et al., 2002a, 2002b). Aiming for promoter elements that are reciprocally active (i.e., can be tested in the rodent) but are likely to function similarly in the primate, we aligned mouse and human genomic DNA and uncovered several *Dlx* domains that were longer than those shared by a wider range of species (Ellies et al., 1997; Ghanem et al., 2003; Sumiyama et al., 2002; Zerucha et al., 2000). rAAVs encoding two of these human sequences were broadly active in primate and rodent forebrain interneurons.

To identify promoters for subclasses of GABAergic neurons, we looked for conserved domains within regulatory regions of genes that are enriched in the respective cell populations. This effort yielded a promoter for targeting somatostatin-positive neurons and another for targeting parvalbumin-positive neurons in the primate and rodent.

We demonstrate that single rAAVs can access forebrain GABAergic neurons broadly and that interdependent viruses can be used to restrict access to specific excitatory and inhibitory subpopulations. Our success suggests that the general strategy of finding DNA sequences that are conserved between rodent and primate and of relying on combinatorial methods to refine genetic targeting is applicable to many neuron classes and will aid the transgenics-independent brain-wide interrogations of functionally significant cell populations.

RESULTS

Targeting GABAergic Neurons in the Rodent and Primate with Single AAVs

From the outset, our goal had been two-fold: to assemble short GABAergic interneuron-specific promoters that could be used in viruses and to maintain promoter specificity across mammalian species, especially in primates, in which genomic manipulations can be especially cumbersome. The developmental fate of forebrain interneurons in many species is determined partly by the products of *Dlx* genes (Cobos et al., 2005, 2007; Long et al., 2009; Stühmer et al., 2002a, 2002b). Several nearby enhancer domains incorporated into transgenic mice (Ghanem et al., 2003; Potter et al., 2009; Stühmer et al., 2002b) and viral

vectors (Dimidschstein et al., 2016; Lee et al., 2014) have previously been shown to restrict reporter expression to forebrain GABAergic interneurons.

Striving to develop promoters that are broadly active in the primate brain, but could be validated in the rodent, we aligned human and mouse *Dlx* genomic DNA *de novo* and identified highly conserved reciprocal domains that were longer than those described previously (Figure 1A). Human sequences were then screened for expression strength and specificity in the mouse forebrain.

Of the three human sequences from the *Dlx1/2* region, a 376 bp segment, termed h12R, was active predominantly in GABAergic interneurons (specificity: HPC 96.3% ± 1.9%, CTX 93.2% ± 0.9%). However, not all GABAergic interneurons were labeled (coverage: HPC 83.4% ± 0.8%, CTX 84% ± 2.8%; Figures 1C–1D). In addition, some neurons were weakly labeled (Figure 1E).

Of the two human sequences from the *Dlx5/6* genomic region, an 836 bp segment, termed h56D, supported reporter expression in nearly all mouse GABAergic neurons (specificity: HPC 94.9% ± 1.0%, CTX 92.8% ± 1.4%; coverage: HPC 91.4% ± 1.1%, CTX 92.8% ± 1.4%; Figures 1F, 1G, and S1C).

Remarkably, in the reverse orientation, h56R was not selective (Figure S1C) but similar to another sequence used in viruses to target GABAergic interneurons (*h/mDlx*; Dimidschstein et al., 2016; Figure 1A).

We then tested whether h56D could restrict transgene expression to GABAergic neurons of another rodent. In the Mongolian gerbil, a popular model for auditory studies, forebrain GABAergic interneurons were also targeted with high specificity (HPC 98.4% ± 1.6%, CTX 83.6% ± 0.4%; Figures 1F and 1G). In contrast, none of the promoters we tested was active in the GABAergic neurons of rodent inferior colliculus (Figure S1D), consistent with their mesencephalic origin and the corresponding lack of *Dlx* gene expression in the midbrain (Bulfone et al., 1993; Lahti et al., 2013). The effectiveness of h56D in mouse and gerbil forebrain suggests that it is broadly applicable in rodent models.

We also confirmed h56D efficacy in the marmoset cortex, where nearly all labeled neurons were GABAergic (specificity 96.5% ± 1.6%). Reporter expression was likewise detected across all cortical layers (coverage 88.0 ± 1.4; Figures 1F and 1G). Robust and stable expression was also observed at eight sites in the visual cortex of four macaque monkeys: direct expression from the h56D promoter was seen at four sites in two macaques, and expression restricted to putative GABAergic interneurons using two viruses was seen at three sites in two additional macaques (Figures S2A and S2B).

To demonstrate that h56D viral vectors could be used to record functional responses from primate cortical interneurons, we expressed GCaMP6f in marmoset area MT (Figure 2A) and rhesus macaque area V1 (Figures S2D and S2E). Two-photon imaging of the marmoset cortex revealed differential visually evoked fluorescence changes in response to distinct motion stimuli (Figure 2B). Wide-field imaging at three injection sites in two macaques likewise uncovered robust fluorescence changes related to the repeated presentations of

visual stimuli (Figures S2E and S2F). These findings buttress our proposition that conserved gene-regulatory elements can support cross-species cell type specificity and can be used to reveal the functional characteristics of primate inhibitory neurons.

Composition of Targeted GABAergic Neuron Pool

Next, we set out to examine the complement of GABAergic neurons accessed by h12R and h56D promoters using *in situ* mRNA probes for parvalbumin (PV), somatostatin (SST), neuro-peptide-Y (NPY), and vasoactive intestinal peptide (VIP), molecular markers for the predominant GABAergic cell populations in the forebrain (Armstrong et al., 2012; Freund and Buzsáki, 1996; Klausberger and Somogyi, 2008; Rudy et al., 2011).

The h12R promoter was active in nearly all mouse PV^+ and SST^+ neurons (Figure 3). However, NPY^+ and VIP^+ coverage was incomplete: NPY^+ neurons were underrepresented throughout the dorsal hippocampus (Figures 3A and 3C); cortical layers 2/3 and 5/6 also contained unlabeled NPY^+ cells (coverage: layer 2/3 90.3% ± 1.7%, layer 5/6 73.3% ± 2.0%), and almost all layer 4 NPY^+ cells were unlabeled (Figure 3C). In the hippocampus, excluded VIP^+ cells were restricted primarily to the pyramidal layer, whereas in the superficial layers of the neocortex (layer 2/3), approximately 25% of VIP^+ cells were not labeled (Figures 3A and 3C). Furthermore, we observed that even within the included neuron populations, expression from h12R was not uniform: unlike PV^+ and SST^+ cells, NPY^+ neurons segregated into clearly distinguishable groups of high and low expressers, perhaps consistent with developmental and functional cell heterogeneity within these GABAergic populations (Gelman et al., 2009; Ascoli et al., 2008; Tricoire and Vitalis, 2012).

In contrast, the h56D promoter supported uniform reporter expression in each of the PV^+, SST^+, NPY^+, and VIP^+ GABAergic cell classes (Figures 3B and 3D). In sum, we constructed two GABAergic interneuron-specific promoters: h56D, which provided genetic access to all interneuron subclasses, and h12R, which provided access to subsets of interneurons. We could now use these promoters to further refine interneuron targeting with set intersection and set difference strategies.

Set Intersection Strategy to Target SST^+ Interneurons

In rodents, SST^+ interneurons account for approximately 30% of cortical GABAergic cells (Freund and Buzsáki, 1996; Jinno and Kosaka, 2006; Rudy et al., 2011). SST^+ interneurons primarily innervate dendritic arbors of principal neurons to regulate excitatory input integration and dendritic excitability (Chiu et al., 2013; Lee et al., 2013; Lovett-Barron et al., 2012, 2014; Muñoz et al., 2017; Pfeffer et al., 2013; Royer et al., 2012; Xu et al., 2013). SST^+ interneurons play key roles in both sensory processing in the neocortex and learning in the hippocampus (Adesnik et al., 2012; Lovett-Barron et al., 2012, 2014). However, tantalizingly little is known about specific roles of SST^+ neurons in primates, as these cells have been largely inaccessible.

To target SST^+ neurons, we identified a candidate regulatory domain upstream of the SST gene that was conserved between mouse and human genomes (ECR Browser, Ovcharenko et al., 2004; Figure 4A). However, the resulting promoter accessed both SST^+ and excitatory

neurons (Figure S3A). We then constructed two interdependent rAAV vectors intending to restrict fluorophore expression from the h56D GABAergic promoter to neurons expressing the Cre recombinase from the SST promoter (Figure 4B). Together, this set intersectional approach using two viruses reliably confined reporter expression to GABAergic SST^+ interneurons in the mouse and gerbil hippocampus and mouse neocortex (mouse HPC 92.3% ± 1.5%, mouse CTX 90.2% ± 1.5%, gerbil HPC 86.7% ± 2.8%; Figures 4C and 4D). SST^+ interneurons at the marmoset cortical layer 2/3 injection site were likewise specifically labeled (marmoset CTX 98.5% ± 1.4%; Figures 4C and 4D). The two-virus mix also functioned in the macaque cortex (Figure S2C), but cell identity in the macaque has not been independently confirmed. The SST^+ neuron targeting strategy also worked when Flp recombinase (Kranz et al., 2010; Raymond and Soriano, 2007) was used in place of Cre (Figure S4), offering the means to access a second cell population in animals that already express Cre, such as in PV-Cre mice (Figure S4B).

We had previously demonstrated a role for hippocampal SST^+ neurons *in vivo* in responding to aversive cues (Lovett-Barron et al., 2014). To evaluate the set intersection approach for functional studies, we introduced GCaMP6f into mouse hippocampus using virus alone and subjected the animals to pseudorandom discrete stimuli consisting of light flashes, tones, and mildly aversive air puffs to the snout (Lovett-Barron et al., 2014). We detected robust GCaMP6f responses in CA1 stratum oriens SST^+ neurons (Figure S9A). Air puffs, but not light flashes or tones, evoked strong responses in most SST^+ cells (Figures S9B and S9C). These observations are consistent with our previous report using *SST-Cre* knockin mice (Lovett-Barron et al., 2014), confirming the suitability of the set intersectional cell targeting strategy—including h56D promoter strength, which here set the level of GCaMP6f expression—for functional imaging.

Set Intersection Strategy to Target PV^+ Interneurons

PV-expressing (PV^+) interneurons represent another major inhibitory subclass in the mammalian cortex and hippocampus. PV^+ basket and axo-axonic cells are key regulators of brain rhythms, and they are intimately involved in the microcircuitry of sensory processing, memory formation, and critical period plasticity (Cobb et al., 1995; Klausberger and Somogyi, 2008). Dysfunction of PV^+ interneurons has been linked to autism and schizophrenia (Lewis et al., 2005).

To identify a promoter that is selectively active in PV^+ interneurons, we first tested a conserved region upstream of the PV gene, a tactic that had worked well in the search for the SST promoter. However, the resulting construct showed little PV selectivity in the mouse brain (Figure S3B).

We then used our recently developed algorithm, SArKS (Wylie et al., 2018), and mined RNA sequencing (RNA-seq) data (Mo et al., 2015) for sequence motifs associated with cell type-specific expression in PV^+ neurons. Among the genes highlighted by SArKS was *PaqR4,* a member of the progestin receptor family (Tang et al., 2005). When tested alone in the mouse hippocampus, rAAV encoding the human *PaqR4* promoter labeled PV^+ neurons but also some excitatory and putative glial cells (Figure S3B). However, an intersectional approach using h56D to refine labeling (Figure 5C), as described above to target SST^+

neurons, displayed high specificity for PV^+ cells in rodent cortex and hippocampus (mouse HPC 79.8% ± 4.9%, mouse CTX 69.1% ± 1.4%, gerbil HPC 76.8% ± 1.3%; Figures 5D and 5E).

Reporter expression was also highly specific in PV^+ neurons of the marmoset cortical area MT (specificity 87.4% ± 1.4%, coverage 87.1% ± 3.5%; Figures 5D and 5E), higher percentages than we saw in the rodent forebrain.

Set Difference Strategy to Target Excitatory Neurons

The targeting of excitatory neurons with viruses is generally achieved using a section of the mouse calcium/calmodulin-dependent protein kinase II alpha (CaMKIIα) promoter (Dittgen et al., 2004). However, under certain conditions, this promoter can also be active in inhibitory interneurons (Nathanson et al., 2009a; Schoenenberger et al., 2016) and inactive in subsets of cortical excitatory neurons (Huang et al., 2014; Wang et al., 2013; Watakabe et al., 2015). Moreover, there is considerable regional variation in the expression of endogenous CaMKIIα in the rodent and primate brains (Benson et al., 1991,1992).

Relying on the broad interneuron specificity of the h56D promoter, we tested a two-virus strategy for accessing excitatory-only neurons by effectively subtracting the inhibitory interneuron population from all neurons (Figures S5A and S5B). The set difference strategy is unlike the set intersection approach in that the vectors are not fully interdependent: the primary vector is active until expression is blocked; an inefficient block results in false positives.

We constructed one viral vector where a *floxed* reporter protein in the forward (sense) orientation was transcribed from a pan-neuronal human synapsin promoter (hSYN-$[EGFP_{FWD}]^{Cre}$) (Borghuis et al., 2011; Schoch et al., 1996). A second vector expressed the Cre recombinase from the h56D inhibitory promoter (h56D-Cre; Figure 6A). When co-injected into the mouse dorsal hippocampus, the virus-encoded recombinase converted the sense reporter orientation to an antisense orientation only in inhibitory interneurons and thus restricted reporter expression to excitatory neurons without relying on the CaMKIIα promoter (11.2% ± 1.0% of $GAD65^+$ cells remained labeled, consistent with neuron coverage when using the h56D promoter; Figure 6B). If GABAergic interneurons account for approximately 10% of mouse hippocampal neurons, we estimate a false-positive rate for the set difference strategy (i.e., that an excitatory cell turns out to be inhibitory) of 1 %–2%.

Set Difference Strategy to Target Subsets of NPY Interneurons

We can also use a set difference strategy to access subsets of NPY^+ interneurons. These are a diverse population in rodents, with respect to both their origin (Fuentealba et al., 2008; Gelman et al., 2009; Miyoshi and Fishell, 2011; Tricoire and Vitalis, 2012) and their function. In addition to modulating individual excitatory neuron firing rates through feedforward inhibition, NPY^+ interneurons form gap junctions with each other and nearby GABAergic cells, potentially coupling cortical networks (Armstrong et al., 2012; Fuentealba et al., 2008; Simon et al., 2005). As a neuropeptide, NPY can also promote neurogenesis (Decressac and Barker, 2012) and acts as an anti-epileptic (Baraban et al., 1997; Noè et al., 2008). Because NPY^+ interneurons had previously only been examined using transgenic

mice (Milstein et al., 2015; van den Pol et al., 2009), we decided to try targeting them using our GABAergic promoters.

We had noted earlier that the h12R promoter demonstrated little to no activity in a significant fraction of NPY^+ neurons (Figures 3A, 3C, and S7B). To examine if differences in h12R versus h56D promoter activity could be harnessed to access functionally distinct subsets of NPY^+ interneurons, we built pairs of interdependent viruses for tunable cell type-specific heterologous protein expression. One vector from each pair contained a tetracycline regulon (TetO4) inserted into the cytomegalovirus minimal promoter (Yao et al., 1998). A tetracycline repressor (TetR; Beck et al., 1982; Hillen and Berens, 1994) was encoded by the second vector (Figure S7A). When cultured fibroblasts were transfected with different ratios of such constructs, TetR blocked reporter expression in a dose-dependent fashion (Figure S6A).

Mixes of h12R and h56D repressor and reporter vectors (respectively) injected into mouse brains labeled high percentages of forebrain NPY^+ neurons (specificity: HPC 89.7% ± 1.3%, CTX 87.9% ± 1.8%). However, in line with the h12R expression pattern (Figure 1C), coverage was incomplete and stratified: NPY^+ neurons were abundant in stratum oriens but largely absent in hippocampal strata radiatum and lacunosum-moleculare (72.6% ± 6.2% versus 27.8% ± 1.6% coverage; Figures 7B and S7E); in addition, cortical layer 2/3 had fewer labeled neurons than layer 5/6 (55.6% ± 6.4% versus 35.4% ± 2.3% coverage; Figures 7C and 7D). In the hippocampus, the few virus-labeled NPY^- neurons were VIP^+ (Figure S7C).

We proceeded to examine the characteristics of the virus-labeled cells and uncovered two subclasses of NPY^+ interneurons. Immunostaining for PV showed that, compared with h56D alone, approximately half of all PV^+ neurons had been labeled by the interdependent viruses, the majority in stratum pyramidale (PV^+ coverage 44.1% ± 6.7%; Figure S8B). The labeled PV^+ neurons were predominantly NPY^+ (86.8% of labeled PV^+ neurons were PV^+/NPY^+), while the unlabeled PV^+ neurons were NPY^- (Figure S8B). Therefore, the NPY^+/PV^+ subclass specificity was high, and the NPY^+/PV^+ coverage was nearly comprehensive (95% ± 8.2% of NPY^+/PV^+ neurons had been labeled by the viruses).

Immunostaining also revealed that the h56D/h12R interdependent viruses labeled less than half of hippocampal SST^+ neurons (SST^+coverage 42.6% ± 7.9%; Figure S8C). However, this entire population comprised SST^+/NPY^+ neurons in stratum oriens (Figure S8C), of which 80% (80.2% ± 8.2% coverage) had been labeled, providing a way to selectively enrich for this subset of interneurons (Jinno and Kosaka, 2004). This population was distinct from the PV^+/NPY^+ neurons described above, consistent with the reported segregation of neocortical PV^+ and SST^+ interneuron subclasses (Rudy et al., 2011).

To demonstrate that we could specifically target the SST^+/NPY^+ interneuron subpopulation, which cannot easily be accessed using transgenic animals, we set up a double restriction in wild-type mice, imposing the SST requirement onto the subset of NPY^+ neurons (Figure S8D). We were thus able to isolate hippocampal SST^+/NPY^+ neurons (coverage 95.6% ± 2.8%; Figure S8E).

Next, we tested if we could examine hippocampal NPY^+ neuron function *in vivo.* Without a template for NPY^+ cell activity during a behavioral task, we settled for a confirmation that subtractive expression of GCaMP6f using the two-virus system supported functional imaging. Stratum oriens, but not stratum pyramidale, neurons expressed abundant GCaMP6f (Figure S9D), and on the basis of preliminary *in vivo* head-fixed two-photon Ca^{2+} imaging, NPY^+ neurons exhibited reliable locomotion-related activity, with subset displaying tight cross-correlation in the activity profiles (Figures S9E and S9F).

Our set difference method for cell type-specific expression regulation represents a proof of concept for a transgenics-independent way to target defined classes of neurons in the brain. Although we used a fixed molar ratio of reporter and repressor vectors to enrich for NPY^+ neurons, different promoters and ratios could access other cell subsets within and across traditional neuron classes for imaging and manipulation. Importantly, unlike recombinase-dependent techniques for expressing foreign proteins, the TetR-dependent approach is selective, tunable, and reversible when regulated using injectable doxycycline or doxycycline added to animal chow (not shown). In addition, the TetR set difference technique can be used orthogonally with recombinases to target two cell classes, or jointly with recombinases, as demonstrated for SST^+/NPY^+ neurons above, to examine previously inaccessible neuronal circuit elements.

DISCUSSION

Accessing neuronal subclasses is essential for unraveling brain circuitry that governs animal perception and behavior. However, functional studies have revealed that the relevant cell ensembles, excitatory or inhibitory, rarely fall within neat neurochemical boundaries (Soltesz and Losonczy, 2018). Moreover, neuronal gene expression is both promiscuous and variable (Cembrowski and Menon, 2018; Lein et al., 2007), making it difficult to find single surrogate markers for the emerging functional classes.

Our effort shows how overlapping endogenous gene expression, normally a hindrance to cellular marker-based genetic targeting, can be overcome and harnessed to access neuronal subclasses. This undertaking was driven by three interrelated hypotheses: (1) that the ability of a subset of neurons to express a reporter from a short promoter is a manifestation of an underlying functional uniformity, (2) that more than one such promoter may be needed to define a homogeneous cell subclass, and (3) that regulatory regions conserved between two species will display similar cell type specificity in both species. Consistent with these hypotheses, we accessed neocortical GABAergic interneurons in rodent and primate using a conserved enhancer domain associated with a developmental programming gene, rather than a traditional interneuron marker. We then used combinations of promoters to target subclasses of GABAergic interneurons, again relying on conserved regulatory domains of co-expressed genes.

We took a comparative approach to uncover sequences that could support heteroprotein expression exclusively in GABAergic interneurons of the mammalian forebrain. Our general strategy was to identify and test sequences likely to be involved in gene expression regulation. Intergenic *Dlx* domains had already been shown to possess this ability in adult

transgenic mice, and some of these sequences appeared to be especially active in GABAergic cells. Because these sequences were enhancers, we tested each in the forward and the reverse orientations. Our efforts yielded a sequence (h56D) that provides uniform protein expression across GABAergic cells. The same sequence in the opposite orientation was ineffective for GABAergic cell targeting. We also uncovered a number of sequences within *Dlx* domains with more complex activity patterns: some supported reporter expression in glutamatergic and GABAergic cells; others were differentially active in GABAergic interneuron subclasses. For SST^+ interneuron targeting we examined the DNA sequence immediately upstream of the SST gene. For PV^+ interneuron targeting we analyzed upstream sequences of genes enriched in PV^+ cells. In both instances, we focused on regions conserved between rodent and primate. Finding sequences appropriate for rodents allowed us to test promoter specificity more quickly. This strategy has helped us to identify additional sequences for refining protein expression to more subclasses of inhibitory interneurons.

On the basis of this initial survey of promoter successes and failures, we derived computational and combinatorial methods for targeting subsets of GABAergic interneurons. In one example, we used a set intersection strategy to show that SST^+ interneurons may be accessed using a combination of the h56D promoter and the conserved domain within the SST promoter. This intersectional technique interlocked the viral vectors, restricting reporter expression only to cells in which promoters encoded by both vectors were active, as neither vector alone could express reporter.

In another example, we developed an algorithm that searched *de novo* for DNA motifs shared by putative promoters of genes expressed in mouse PV^+ neurons but not VIP^+ or excitatory neurons (Wylie et al., 2018). Many of the uncovered motifs were not present in repositories of transcription factor binding sites (Khan et al., 2018). We then selected a small subset of gene regulatory regions that contained such motifs, were substantially conserved across species, and were not under epigenetic control, which might override sequence-dependent regulation and would be impossible to reproduce when using an episomal viral vector. *PV* gene itself was excluded on the basis of its differential chromatin accessibility (Mo et al., 2015), and indeed, the putative *PV* regulatory region turned out not to support cell type-specific reporter expression. However, the promoter from human *PaqR4,* one of the top SArKS candidates, was active in the majority of PV^+ neurons. By selecting a gene other than *PV*, we were certain to miss some PV^+ neurons; moreover, we anticipated needing an additional restriction, provided here by h56D. However, we reasoned that given the heterogeneity of the PV^+ and other major interneuron classes, our aim was not to achieve comprehensive coverage but to strive for functionally homogeneous interneuron subclasses. The choice of human sequence may also have contributed to the higher targeting specificity of PV^+ neurons in the marmoset cortex than in rodent.

We used another set difference strategy to enrich for subsets of NPY^+ interneurons. In this case, we restricted expression from the inhibitory h56D promoter to cells in which a second, less general h12R promoter was inactive using a modified TetR system. The specific subsets of NPY^+/SST^+ and NPY^+/PV^+ interneurons have heretofore been inaccessible using transgenic animals or viral techniques.

In another example of the set difference strategy, we were able to isolate hippocampal excitatory or inhibitory neurons by subtracting cells accessed by an inhibitory or an excitatory promoter, respectively, from those accessed by a pan-neuronal promoter. This may be a useful approach in subcortical regions in which the excitatory or the inhibitory promoter proves unreliable, as we observed with h56D in the rodent midbrain, and cannot be used directly.

Combinatorial strategies depend on co-infection of neurons by multiple rAAVs. The high titers and broad infectivity of our viruses substantially increase the likelihood of co-infection. However, if co-infection does not occur, the outcomes for our two combinatorial strategies will be different. In set intersection, the individual viruses are not functional separately and failed co-infection will result in false negatives: cells that should have been labeled but are not. However, set difference relies on blocking ongoing gene expression. As a result, infection only by the primary reporter-producing construct, but not the blocker, will yield a false positive: an inappropriately labeled neuron.

To test the limits of co-infection, we injected virus mixes that either expressed different color reporters from similar promoters (Figure S6) or that were needed to target NPY^+ neurons (Figure S7D). We then tiled injection sites for analysis, comparing reporter overlap and targeting specificity at injection site centers versus their edges. For both direct reporter coexpression and the set difference strategy to label NPY^+ neurons, we found that variability in fluorophore overlap was negligible (Figure S6) and targeting specificity was within the margin of error across injection sites: injection site edges could be less brightly labeled, but specificity was maintained (Figure S7D). Not finding a clear drop-off in co-infection and specificity was surprising, as we had hypothesized that cells at an edge of a labeled brain region are more likely to be infected by a single viral construct. An explanation may be that multiple viral particles must infect a neuron for resulting fluorescence to be detected, such that neurons infected by very few particles require immunostaining or another signal amplification technique to be seen. If this is the case (i.e., that all visualized neurons had been infected by multiple viruses), co-infection, and for NPY^+ neuron targeting the ratio of operator to repressor, would be maintained even as the overall virus concentration drops, preserving targeting specificity.

These multi-virus techniques for accessing key subsets of neurons represent viable alternatives to single cell type-specific promoters and provide ample protein expression for nuanced functional studies, including *in vivo* imaging and manipulation studies in the primate, of the diverse cell populations that comprise the cortex and hippocampus. Indeed, bringing methods that have enabled breakthrough examinations of rodent neural circuit mechanisms to the primate has been a priority for our laboratories. Our techniques can also be combined to further refine cell targeting or used orthogonally in circuit-level experiments. These general methods offer a timely blueprint applicable to many neuron classes and species that will aid the transgenics-independent brain-wide interrogations of functionally significant cell populations.

STAR★METHODS

CONTACT FOR REAGENTS AND RESOURCES

Requests for reagents and resources should be addressed to and will be fulfilled by the Lead Contact, Boris Zemelman (zemelmanb@mail.clm.utexas.edu).

EXPERIMENTAL MODEL AND SUBJECT DETAILS

All experiments were conducted in accordance with the National Institutes of Health guidelines and with the approval of the University of Texas at Austin and Columbia University Institutional Animal Care and Use Committees.

Mice—Male and female C57BL/6J, 129S and Ai14 (Madisen et al., 2010) mice (8-16 weeks) were obtained from The Jackson Laboratory (Bar Harbor, ME) and bred in-house. NPY-Cre (Milstein et al., 2015) and PV-Cre (Scholl et al., 2015) were generated and bred in-house. PV-Cre;Ai14 mice were bred in-house. Mice were housed in groups of up to 4 animals and maintained on a 12 h reversed light/dark cycle. Surgeries and imaging experiments were conducted during the dark phase. Food and water were provided *ad libitum,* except as indicated below for *in vivo* imaging studies.

Mongolian gerbils—Male and female gerbils (3-5 weeks) were obtained from The Jackson Laboratory (Bar Harbor, ME) and bred in-house. Gerbils were housed in groups of up to 6 animals and maintained on a 12 h light/dark cycle. Food and water were provided *ad libitum*.

Non-human primates—Male and female marmosets (1.5-4 years) were obtained from TxBiomed and bred in-house. marmosets were group-housed. Male macaques (5-10 years) were obtained either from Covance SA (Texas) or the University of Louisiana; they were pair-housed at the Animal Resource Center of the University of Texas at Austin. Food and water were provided *ad libitum* to all primates.

Cell culture: HEK293T cells were obtained from ATTC and propagated according to standard methods. Briefly, cells were grown at5% CO_2 in DMEM supplemented with 10% (v/v) FBS, 2 mM l-glutamine and penicillin/streptomycin to 50%–80% confluence (GIBCO-BRL). Cell were transfected using jetPEI reagent (VWR) as recommended by the manufacturer. Indicated plasmid DNA mixes were incubated with transfection reagent in a 3:1 ratio. The cells were imaged 12-24 h post-transfection on an AXIOZoom V16 fluorescence microscope (Zeiss).

METHOD DETAILS

AAV vector assembly and production—To prepare the hybrid promoters, each genomic enhancer domain was amplified by PCR from human genomic DNA and cloned in front of a cytomegalovirus (CMV) minimal promoter as a Not1-Nsi1 fragment. PCR primers containing these restriction enzyme sites were used to specify enhancer orientation within the construct. Enhancer sequence boundaries were as follows:

h12a — GAAAGAGGTCCCCAGGACCA … CCAAGGCAAATTTTCACTGT

h12LR — GCAAAATCTGTTTGGTCAAG … AAATTGCCAAACAACAGATA

h12R — CAGCTGCAAACCCAAGAGGG … AAATTGCCAAACAACAGATA

h56D — AGAAATAATGAAAATGAAAA … TTGCTGAATTATTCAAATTA

h56ii — TCTGAGTCTCAGGGCAGAAG … AGCAAATCAGTGGTCTGAAG

To achieve TetR regulation, the CMV minimal promoter (GGGGGTAGG … GATCGCCTG) was interrupted by tandem palindromic TetO binding sites (TCCCTATCAGTGATAGAGA) (Hillen and Berens, 1994) separated by two base pairs (TC) starting 10 base pairs after the CMVTATA box (Yao et al., 1998). All h56D vectors contained TetO binding sites. TetO sites were not present in vectors expressing TetR. The CMV minimal promoter was cloned as Nsi1-Sac1 fragment, such that all hybrid promoters were delimited by Not1-Sac1 sites. The SST promoter (CCAGATCAA … GCAAGGAAG) was amplified from mouse genomic DNA. The human PaqR4 promoter (GGAAGGGGA … GGAGAGACT) was synthesized *de novo* (Integrated DNA Technologies). The 1.3 kb CaMKIIα promoter (AATTCATTA … GGCAGCGGG) has been described previously (Dittgen et al., 2004). The CMV minimal promoter was not used with SST, PaqR4 or CaMKIIα promoters, which were all cloned as Not1-Sac1 fragments. Genes: EGFP, tdTomato, iCre (Shimshek et al., 2002), Flpo (Kranz et al., 2010; Raymond and Soriano, 2007) and TetR (Yao et al., 1998), each preceded by a Kozak sequence were cloned immediately behind a promoter as Sac1-Pst1 fragments. To impose recombinase dependence, the Kozak-gene cassette was inserted between asymmetric optimally-spaced *loxP* or *frt* recombination sites (Schlake and Bode, 1994; Seibler and Bode, 1997). In each viral construct, the promoter, gene, woodchuck post-transcriptional regulatory element (WPRE) and SV40 polyadenylation sequence were flanked by two inverted terminal repeats. Viruses were assembled using a modified helper-free system (Stratagene) as serotypes 2/1 or 2/7 (*rep/cap* genes). Serotype choice did not affect targeting specificity. Viruses were purified on sequential cesium gradients according to published methods (Grieger et al., 2006). Titers were measured using a payload-independent qPCR technique (Aurnhammer et al., 2012). Typical titers were > 10^{10} genomes/microliter.

Stereotaxic injections—Mouse: Both male and female mice were used for promoter characterization and slice electrophysiology studies. Only male mice were used for *in vivo* imaging studies. Mice were anesthetized with inhaled isoflurane (1%–5% in oxygen), and body temperature was maintained at 37°C. Injections were performed using a stereotaxic apparatus (Kopf) fitted with a Nanoject II microinjector (Drummond Scientific). Pulled-glass pipettes back-filled with mineral oil were used to deposit virus mixes. For promoter characterization ~20 nL virus was deposited bilaterally in hippocampal CA1 at depths 100 nm apart (from bregma: AP −2.2 mm; ML ± 1.5 mm; D −1.8 mm to −0.8 mm). For *in vivo* imaging studies, ~30 nL virus was injected at six sites within the left CA1 region in three 10 nL pulses per site (from bregma: AP −2.2 mm; ML +1.5 mm; D 1.2, 1.1, 1.0 mm; and AP −2.5 mm; ML +1.6 mm, D 1.2, 1.1, 1.0 mm). Cortical injections were performed using a Micro4 controller (World Precision Instruments) to deposit ~200 nL virus at the rate of 10 nl/min at a single location (from bregma: AP −2.2 mm; ML ± 1.5 mm; D −0.3 mm). Pipettes were left in place for 10 min following the injections. Animals were allowed to recover for at least 10 days post-injection. **Gerbil:** Gerbils of both sexes underwent stereotaxic surgery

for virus injection at 3-5 weeks of age. Gerbils were anesthetized with inhaled isoflurane (1%–3% in oxygen), and body temperature was maintained at 37°C. Injections were performed using a stereotaxic apparatus (Kopf) fitted with a Nanoject II microinjector (Drummond Scientific). Pulled-glass pipettes back-filled with mineral oil were used to deposit virus mixes. In the inferior colliculus, 50 nL of virus was deposited bilaterally at depths 200 nm apart (from lambda: AP −1.25 mm; ML ± 1.15 mm; D −3.2 mm to −2.8 mm). In the hippocampus, 30 nL of virus was deposited bilaterally at depths 200 nm apart (from bregma: AP: −2.8 mm; ML: +1.8 mm; D: 1.6 mm to 0.2 mm). Cortical injections were performed using a Micro4 controller (World Precision Instruments) to deposit 200 nL of virus at the rate of 10 nL/min (from bregma: AP: −2.8 mm; ML: +1.8 mm; D: −0.3 mm). Pipettes were left in place for 10 min following the injections. Animals were allowed to recover for at least 10 days post-injection in group housing. **Marmoset**: Adult marmosets were anaesthetized with isoflurane and placed in a stereotaxic frame. The body temperature was maintained at 36-37°C and the heart rate, spO_2 and CO_2 were monitored throughout the procedure. The head was disinfected, and the surgery was performed under sterile conditions. A circular craniotomy of 4 mm diameter was performed on the cortex and the dura was removed. The virus was injected using Nanoject II (Drummond Scientific) with pulled and beveled glass pipettes with a tip diameter of 20-35 μm. The glass pipette was filled with mineral oil and front-loaded with the virus. The pipette was lowered into the visual cortex (D −0.5mm). The virus was injected at 23 nl/sec up to a volume of 500 nl. The pipette was left in place for 5 min. Injection spread was assessed using trypan blue diluted 1:5 in virus mix. The craniotomy was closed using a custom-made chamber. The animals were then returned to their cages. Downstream procedures were conducted after a recovery period of 4-5 weeks. **Macaque:** Surgical procedures, injection and expression screening were performed as described previously (Seidemann et al., 2016). After viral injection, widefield epifluorescence images of injection sites were taken weekly until the chamber was removed (see Seidemann et al., 2016). Red fluorescent protein (tdTomato) was imaged using 540 nm excitation and 565 nm dichroic filters. Green fluorescent protein (EGFP) was imaged using 470 nm excitation, 505 nm dichroic, and 520 nm emission filters.

For virus co-injections, the viruses were titer-matched and used in a 1:1 ratio (h12R-tdTomato:h12D-EGFP, SST-Cre:h56D-$(EGFP)^{Cre}$, SST-Flp:h56D-$(EGFP)^{Flp}$, PaqR4-Cre:h56D-$(EGFP)^{Cre}$), 1:2 ratio ($h56D_{TetO4}$-tdTomato:h12R-TetR and $h56D_{TetO4}$-GCaMP6f:h12R-TetR), 1:1:2 ratio ($h56D_{TetO4}$-tdTomato:hSYN-$(EGFP)^{Cre}$:h12R-TetR) and (SST-Cre:$h56D_{TetO4}$-$(EGFP)^{Cre}$: h12R-TetR), 1:2 ratio (hSYN-$(EGFP_{FWD})^{Cre}$:h56D-Cre) and (hSYN-$(EGFP_{FWD})^{Cre}$:CaMKIIα-Cre).

GABAergic neuron targeting—To develop short GABAergic interneuron-specific promoters that could be used in viruses and that would maintain their specificity across mammalian species, we initially focused on the *Dlx* gene clusters. The developmental fate of forebrain interneurons in many species is partly determined by the products of *Dlx* genes (Cobos et al., 2005; 2007; Long et al., 2009; Stühmer et al., 2002a; 2002b), the vertebrate counterparts of the *D. melanogaster distal-less* homeobox proteins. *Dlx1-6* genes are arranged in bigene clusters interrupted by intergenic regions that contain highly conserved enhancer-like domains, each several hundred base pairs in length (Ellies et al., 1997;

Ghanem et al., 2003; Sumiyama et al., 2002; Zerucha et al., 2000). Rodent and zebrafish variants of these domains incorporated into transgenic mice (Ghanem et al., 2003; Potter et al., 2009; Stühmer et al., 2002b) have previously been shown to support reporter expression in GABAergic interneurons. In addition, two recent studies described interneuron-specific viral vectors containing similar regions (Dimidschstein et al., 2016; Lee et al., 2014).

Striving to develop promoters that are likely to be active in the primate brain, but could be initially tested in the rodent, we aligned human and mouse *Dlx1/2* and *Dlx5/6* genomic DNA *de novo* and identified highly conserved reciprocal domains that were longer than those described previously (Figure 1A). We constructed hybrid promoters by pairing each enhancer domain with a cytomegalovirus minimal promoter. The resulting regulatory sequences were incorporated into rAAV vectors encoding fluorescent reporter proteins (Figure 1B) and were initially evaluated for expression strength and specificity in the mouse hippocampus and cortex.

We tested three human sequences from *Dlx1/2;* as in previous reports (Ghanem et al., 2003), all were in the reverse orientation with respect to their placement within chromosomal DNA. A promoter containing the human variant of the *ml12a* domain, h12a (Figure 1A), labeled mostly inhibitory interneurons, but also some excitatory cells (data not shown), and was not characterized further.

We also tested two promoters incorporating human domains from the *Dlx1/2-ml12b* region (Ghanem et al., 2003): the longer one, the 1000 base pair h12RL, covered the full extent of the human/mouse sequence conservation; the shorter 376 base pair sequence, termed h12R, aligned more closely with the core conserved region at this genomic location (Ghanem et al., 2003), Figure 1A). Both promoters supported reporter expression in similar numbers of cells. Likewise, expression pattern for each promoter in the mouse hippocampal area CA1 was broadly consistent with successful GABAergic interneuron targeting: most labeled cells were located in *stratum oriens,* while only a few appeared in *stratum pyramidale* (Figure S1A). Based on these initial observations, we concluded that the significantly longer h12RL did not confer a clear cell type-specific expression benefit.

We proceeded to characterize the shorter h12R promoter in mouse cortex and hippocampus. Promoter properties were not affected by enhancer orientation, as judged by injecting a mix of two viruses encoding different color reporters (h12R-tdTomato, h12D-EGFP) into the mouse dorsal hippocampus (Figure S1A). More generally, this experiment demonstrated the high likelihood of individual neuron co-infection by multiple viruses, a feature we confirmed in follow-up experiments (Figure S6). We then examined the strength and specificity of the h12R promoter using *in situ* probe hybridization to reporter mRNA and confirmed that it was active predominantly in rodent GABAergic interneurons, however not all GABAergic interneurons had been labeled (Figures 1C and 1D). In addition, among the labeled neurons, a clear subset (~35%) were weakly labeled (Figure 1E).

Trying to increase the proportion of targeted interneurons, we tested several conserved domains identified within the *Dlx5/6* genomic region. The human domain overlapping *ml56ii* (Ghanem et al., 2003) (h56iiD, h56iiR, Figure 1A) was inactive in the rodent brain

irrespective of orientation (Figure S1B), and was not characterized further. Consistent with our findings, previous reports using the zebrafish *zI46ii* domain in transgenic mice indicated inefficient reporter expression in the embryonic forebrain (Zerucha et al., 2000).

In contrast, the h56D promoter, incorporating 836 base pairs of human DNA encompassing and extending beyond the conserved *ml56i* region (Ghanem et al., 2003), supported reporter expression in nearly all mouse GABAergic interneurons (Figures 1F, 1G, and S1C). No reporter expression from the h56D promoter was observed in hippocampal excitatory pyramidal neurons.

Remarkably, in the reverse orientation, h56R labeled both excitatory and inhibitory neurons (Figure S1C). While the h56R promoter partially overlapped and was oriented similarly to *h/mDlx* (Dimidschstein et al., 2016; Figure 1A), the apparent discrepancy in specificity may be due to differences in the sequences of the two promoters.

SST neuron targeting—To target SST^+ neurons, we identified a candidate 2000 base pair regulatory domain just upstream of the mouse SST start codon that was conserved between mouse and human genomes (ECR Browser, Ovcharenko et al., 2004; Figure 4A). ECR Browser settings: domain length 100, similarity cutoff 50. Additional more distant conserved domains were also detected. Selected promoter region extended ~2000 base pairs upstream of the SST start codon, covering three conserved domains. The resulting vector, SST-EGFP, expressed the fluorophore in SST^+ GABAergic interneurons, but also in dorsal CA1 excitatory neurons (Figure S3A). We then constructed two additional interdependent vectors, SST-Cre and h56D-$(EGFP)^{Cre}$, intending to restrict fluorophore expression from the h56D GABAergic promoter to neurons expressing the Cre recombinase from the SST promoter (Figure 4B). Together, this *set intersectional* approach using two viruses reliably confined reporter expression to GABAergic SST^+ interneurons in the mouse and gerbil hippocampus and mouse neocortex (Figures 4C and 4D), the marmoset cortex (Figures 4C and 4D), and the rhesus macaque cortex (Figure S2C), although cell identity in macaque has not been independently confirmed. The SST^+ neuron targeting strategy also worked when Flp recombinase (Kranz et al., 2010; Raymond and Soriano, 2007) was used in place of Cre (SST-Flp and h56D-$(EGFP)^{Flp}$ vectors; Figure S4), offering the means to access a second cell population in parallel with a Cre-dependent system (Figure S4B).

PV neuron targeting—To identify a promoter that is selectively active in PV^+ interneurons, we first tested a conserved region upstream of the *PV* gene, a tactic that had worked well in the search for the SST promoter. However, the resulting construct showed little PV selectivity in the mouse brain (Figure S3B).

We then set out to develop a general and rational approach for promoter candidate selection that aimed to minimize the hit-or-miss aspect of existing strategies. Our goal was to apply our recently developed Suffix Array Kernel Smoothing algorithm, (SArKS; Wylie et al., 2018), that was designed to mine the growing body of RNA-seq data for sequence motifs associated with cell type-specific gene expression.

To identify candidate promoters for accessing PV^+ interneurons, we re-analyzed a mouse RNA-seq dataset (Mo et al., 2015), where Cre recombinase-expressing mice were bred with a Cre-dependent fluorescent reporter mouse strain (Ai14; Madisen et al., 2010) to tag and isolate neocortical excitatory neurons, PV^+ neurons and VIP^+ neurons. First, we used Kallisto (Bray et al., 2016) to localize transcription start sites (TSSs) for the expressed genes. Kallisto reported 73,912 distinct transcripts detected with nonzero estimated count in at least one of the analyzed samples. After filtering out transcripts that had low estimated counts or low average or low variance in transcripts-per-million (TPM) normalized expression levels, 29,164 distinct transcripts remained; these transcripts represented 11,857 distinct genes. We retained only the single transcript variant having the highest average TPM for each gene. For each of the remaining transcripts, we checked whether or not the TSS was located within a chromatin-accessible region in each of the neuron classes (as measured by ATAC-seq; Mo et al., 2015). In order to focus on those genes for which expression variability between neuron classes is most likely to be a function of promoter sequence as opposed to chromatin state, we eliminated all genes where the TSS was not contained within a chromatin-accessible region in every neuron class. The *PV* gene itself fulfilled most of the enumerated criteria, but its chromatin was differentially accessible (Mo et al., 2015); the *PV* promoter was consequently eliminated from contention. The upstream regions (~3 kb) of the remaining 6,326 genes were examined using SArKS (Wylie et al., 2018) to find motifs (k-mers) whose occurrence in a set of promoter sequences correlated with an input metric of differential expression: a t-statistic comparing the TPM-normalized RNA transcript abundance in PV^+ neurons versus PV^- neurons. SArKS first identified motifs by employing smoothing over subsequences by sequence similarity and then identified multi-motif domains (MMDs) by additionally smoothing over spatial proximity, using a permutation testing approach to establish statistical significance. We then used the counts of how many times each uncovered motif occurred in a promoter region as the feature vector for training a regression model to predict differential expression, again quantified as a t-statistic. The predicted scores from this regression model were then used to rank promoters by SArKS motif content, yielding 11 putative regulatory domains for experimental testing, one of which was for *PaqR4* a member of the progestin receptor family (Tang et al., 2005). *PaqR4* transcript was more abundant in PV^+ neurons compared to VIP^+ neurons but was not among the most abundant transcripts (Figure 5A). Its expression pattern in the mouse forebrain is similar to that of *PV* (Allen Brain Atlas, Lein et al., 2007). Its putative regulatory region is fairly short, ~1 kb, and mostly conserved between mouse and human (Figure 5B). When tested alone in the mouse hippocampus, rAAV encoding the human *PaqR4* promoter labeled PV^+ neurons, but also some excitatory and putative glial cells (Figure S3B). However, an intersectional approach using h56D to refine labeling (Figure 5C), as described above to target SST^+ neurons, yielded a highly enriched population of PV^+ cells in rodent and primate forebrain (Figure 5).

NPY neuron targeting—In developing a strategy to target NPY^+ interneurons, we had noted that the h12R promoter labeled approximately 85% of GABAergic neurons in the mouse cortex and hippocampus (Figures 1C and 1D) and that many of the excluded cells were NPY^+ and VIP^+ (Figures 3A and 3C). Moreover, nearly half of NPY^+ neurons targeted by h12R (39.1 ± 5.5%) expressed the reporter weakly (Figure S7B). Thus, h12R promoter

demonstrated little to no activity in a significant fraction of NPY^+ neurons. Based on these observations, we tested combinatorial methods for targeting subsets of NPY^+ interneurons, which have heretofore been inaccessible using transgenics or viral approaches.

Differential promoter activity, such as that seen for h12R, is consistent with recent reports that gene expression variations across cortical and hippocampal interneuron subclasses represent distinctions in degree rather than distinctions in kind (Földy et al., 2016; Harris et al., 2017; Mo et al., 2015; Paul et al., 2017; Tasic et al., 2016; Zeisel et al., 2015). Gradations in gene expression have likewise been detected within relatively homogeneous cell classes, such as among hippocampal excitatory neurons (Cembrowski et al., 2016; Thompson et al., 2008, but see Lein et al., 2007). These studies support the notion that transcriptome variations underlie functional heterogeneity within traditional neuron classes, but also challenge efforts to group and target specific neurons based on single distinguishing genetic markers.

To examine if differences in h12R versus h56D promoter activity could be harnessed to access functionally distinct subsets of NPY^+ interneurons, we used pairs of interdependent viruses for tunable cell type-specific heterologous protein expression. One vector from each pair contained a tetracycline regulon—a dimerized tetracycline operator (TetO4) inserted into the cytomegalovirus minimal promoter (Yao et al., 1998). This operator was already incorporated into all h56D constructs. A tetracycline repressor (TetR, Beck et al., 1982; Hillen and Berens, 1994) was encoded by the second vector (Figure S7A). This scheme is different from the better known $Tet_{ON/OFF}$ systems (Gossen and Bujard, 1992; Gossen et al., 1995), where the repressor acts as a transcription factor, in that here the repressor can block read-through from any TATA box-containing promoter, preserving cell type-specific expression for both reporter and repressor. Moreover, unlike Cre recombinase-dependent schemes, which employ an enzyme and are therefore more difficult to regulate, TetR blocks transcription stoichiometrically, a useful property for exploiting promoter strength variations. Indeed, when we tested our TetR system in cultured fibroblasts transfected with different ratios of reporter and repressor constructs, TetR blocked reporter expression in a dose-dependent fashion (Figure S6A).

To characterize NPY^+ neurons where the h12R and h56D promoters are differentially active, mixes of $h56D_{TetO4}$-tdTomato (the TetO4 designation has been added for clarity, as all h56D constructs already contained this operator within the CMV minimal promoter), h12R-TetR and hSYN-$(EGFP)^{Cre}$ vectors were injected into brains of knock-in *NPY-Cre* mice (Milstein et al., 2015). The hSYN-$(EGFP)^{Cre}$ labeled the endogenous NPY^+ neurons green, while the inhibitory viruses additionally labeled a subset of neurons red (Figure 7A). TetR blocked reporter expression in neurons where the h12R and h56D promoters were comparably active (most $EGFP^-/tdT^+$ GABAergic interneurons), but not in inhibitory cells where h12R promoter was weakly active or inactive ($EGFP^+$ neurons, Figure S7B), such that approximately 90 percent of hippocampal and 88 percent of cortical interneurons labeled by the interdependent viruses were NPY^+ ($EGFP^+/tdT^+$, Figures 7B–7D and S7B).

To demonstrate that we could specifically target the SST^+/NPY^+ interneuron subpopulation, which cannot easily be accessed using transgenic animals, we set up a double restriction in

wild-type mice. We co-injected rAAVs SST-Cre, h56D$_{TetO4}$-(EGFP)^{Cre} and h12R-TetR, imposing the SST requirement onto the subset of NPY^{+} neurons (Figure S8D). With this cocktail, we were able to reliably isolate the SST^{+}/NPY^{+} neurons in the mouse hippocampus (95.6 ± 2.8% of SST^{+}/NPY^{+} neurons had been labeled, Figure S8E).

***In situ* hybridization—**Multiplexed *in situ* hybridization to indicated transcripts were performed using the RNAscope system (Advanced Cell Diagnostics). Whole brains from injected rodents were flash-frozen in OCT medium (Tissue Tek) using a dry ice/ethanol bath at 10-15 days post-injection. Cortical tissue from marmoset visual cortex was collected using a 4 mm biopsy punch (Integra) and immediately flash-frozen in OCT. All samples were cryosectioned at 12 μm (Leica CM3050S) and processed according to probe manufacturer instructions. Briefly, fixed and dehydrated sections were co-hybridized with proprietary probes (Advanced Cell Diagnostics) to neuronal marker transcripts, followed by differential fluorescence tagging. Signals in cells identified using DAPI staining were co-localized on an AXIOZoom V16 microscope (Zeiss).

Immunostaining—Immunohistochemistry was performed on 50 μm sections of fixed mouse and marmoset brain and on 25 μm sections of fresh-frozen marmoset brain. Mice were sacrificed with an overdose of ketamine/xylazine, perfused with PBS, then 4% formaldehyde/PBS. Perfused brains were post-fixed overnight in 2% formaldehyde/PBS, then rinsed and stored in PBS until sectioned on a VT1000S vibratome (Leica). For PV staining, marmoset brain was fixed for 48 hours in 4% formaldehyde/PBS, then rinsed and stored in PBS until sectioned. For SST staining, flash-frozen marmoset tissue in OCT was sectioned on a CM3050S cryostat (Leica), mounted on Superfrost Plus glass slides (Fisher Scientific), and fixed using ice-cold acetone for 10 min. Free-floating mouse and marmoset sections (for PV staining) were permeabilized with 0.5% Triton X-100/PBS and rinsed in PBS. All sections were blocked for 1 h in 5% Normal Goat Serum/0.3% Triton X-100/PBS, then incubated 48 h at 4°C with the indicated primary antibody diluted in blocking solution: rabbit anti-PV at 1:300 (Swant, PV-25/28) and rat anti-SST at 1:200 (Millipore, MAB354). The sections were washed three times with PBS and incubated with Alexa-conjugated secondary antibody (Invitrogen) at 1:500 in blocking solution. The sections were again washed in PBS and mounted on Superfrost Plus glass slides (Fisher Scientific) using DAPI Fluoromount-G (SouthernBiotech). Sections were examined on an AXIOZoom V16 fluorescence microscope (Zeiss); images were acquired on a TCS SP5II laser confocal microscope (Leica). Due to the thickness of the tissue, it was not always possible to accurately determine the number of cells in each field of view using DAPI staining.

In vivo imaging

Rodents: Wild-type mice were injected as described above. Following a 3-5-day recovery period, they were surgically implanted with a cylindrical imaging window—a 3 mm coverslip (Warner) glued (Norland, optical adhesive) onto a 3.0×1.5 mm steel cannula—and a steel head post to facilitate head-fixed imaging experiments. The surgical protocol was performed as previously described (Kaifosh et al., 2013; Lovett-Barron et al., 2014). rAAV vectors SST-Cre and h56D-(GCaMP6f)^{Cre} were used to image SST^{+} interneurons; rAAV

vectors h56D$_{TetO4}$-GCaMP6f and h12R-TetR were used to image NPY^{+} interneurons. Viral expression was assessed through the implanted window starting two weeks post-injection.

Behavioral training: After recovery from surgery, mice were water-restricted (> 85% pre-restriction weight was maintained) and habituated to head fixation under the two-photon microscope. Mice were trained to run on a fabric treadmill for water rewards. Following run training, animals were given a single session (~1200 s) of discrete pseudorandom stimulus presentations while neural activity was monitored with two-photon calcium imaging. Ten stimuli each (tone: 200 ms, 5 kHz, 80 dB; blue LED: 100 ms; air-puff to snout: 100 ms) were delivered using a microcontroller system (Arduino) and custom written software, with a randomized inter-stimulus interval of 10-20 s. Mouse velocity was inferred from belt displacement digitized via and optical rotary encoder (Bourns Inc, ENS1J-B28-L00256L) attached to a microcontroller (Arduino).

Two-photon imaging: Imaging was performed using a two-photon microscope equipped with an 8kHz resonant scanner (Bruker), controlled by Prairie View Software. The light source was a tunable femtosecond pulsed laser (Coherent) running at 920 nm. The objectives were either a Nikon 40 × NIR or a Nikon 16 × water-immersion (0.8 NA, 3.5mm WD and 0.8 NA, 3.00 WD, respectively) in distilled water. Green fluorescence was detected with a GaAsP PMT (Hamamatsu Model 7422P-40); the signal was amplified with a custom dual stage preamp before digitization (Bruker). Images were acquired at 300 μm × 300 μm (512 × 512 pixels) field of view at 30Hz (70-100 mW of power after the objective). Imaging data was motion corrected with a 2D Hidden Markov Model (Kaifosh et al., 2014). Segmentation was performed manually by drawing polygons around the somata of neurons expressing calcium reporter (GCaMP6f). Fluorescence signals were extracted as the average of all pixels within each polygon and relative fluorescence changed were calculated as described (Jia et al., 2011), with a uniform smoothing window t_1 = 10 s and baseline t_1 = 100 s.

Marmosets—Marmosets were injected with viral constructs as described above. The custom-made chamber included an insert with a coverglass at the bottom for optical access to the brain over the stereotaxic coordinates of area MT. In another sterile procedure a custom-made head post was also affixed to the skull using Metabond (Parkell, New York) (Mitchell et al., 2015).

Behavioral training and experimental control: After recovery from surgery, marmosets were food-restricted and habituated to head fixation under the two-photon microscope and trained to fixate visual targets (Mitchell et al., 2015). Experimental control was provided by the Maestro software suite, which collected eye movement data, controlled visual stimulation, and provided juice reward (https://sites.google.com/a/srscicomp.com/maestro/).

Two-photon imaging: Viral expression was assessed by measuring fluorescence beginning 3 weeks after injection using a custom-made two-photon microscope equipped with resonant mirrors to allow for video rate sampling (Scholl et al., 2017). Fluorescence was detected using standard PMTs (R6357, Hamamatsu, Japan) and then amplified with a high-speed current amplifier (Femto DHPCA-100, Germany). Images were acquired at 400 μm × 400

μm fields of view using a 16× objective (Nikon N16XLWD-PF, Japan). Imaging data were motion corrected using cross correlation (Guizar-Sicairos et al., 2008).

Macaques

Wide-field imaging: Four rhesus macaques were injected at 11 sites as described above and evaluated weekly. Static imaging was performed at eight sites in four animals. Fluorescence was detected 2-5 weeks post-injection, images were taken 5-8 weeks post-injection. GECI recordings were performed at 3 sites in 2 animals. Signal could be detected 6-7 weeks post-injection, which was similar to the signal onset observed when using the CaMKIIα promoter (Seidemann et al., 2016). Reliable signal has been recorded for up to 4 months. To date, imaging has been terminated only due to the deteriorating health of one chamber, rather than loss of reporter, and all animals are still being used in experiments. Therefore, no direct histological confirmation of cell type-specificity is yet available in macaques. To evoke a strong visual response in the primary visual cortex (V1), we used a large (6×6 deg^2) sine wave grating at 100% contrast centered at (2.5-3.5) deg, which covered the retinotopic location of the infected area in V1 (0.5-1.0 deg). The stimulus had a spatial frequency of 2 cpd and orientation of 90 degrees. The mean luminance of the screen was set at 30 cd/m^2. The grating was flashed with a temporal frequency of 4 Hz, (100 ms on, 150 ms off) while the monkey was performing a fixation task. The behavioral task and widefield GCaMP data analysis in the macaque were performed as described previously (Seidemann et al., 2016).

QUANTITATION AND STATISTICAL ANALYSIS

Promoter specificity was examined using immunofluorescence and multiplexed *in situ* hybridization. For each experiment, cell counts were obtained from 2-3 mice and 2 gerbils injected bilaterally, as indicated in figure legends. For primate studies, we used 4 marmosets injected at multiple sites, one animal for each targeting and imaging experiment, and we used a total of 4 rhesus macaques injected at multiple sites with multiple vectors for measurements of static fluorescence and for wide-field imaging experiments. Direct fluorescence analysis was performed during the initial examination of all viral vectors to locate the injection site, and it was followed by immunofluorescence or *in situ* studies. A typical injection field covered up to 1 mm of brain tissue. For fluorescence analysis, twenty-four 50 μm tissue sections were collected per injection site per hemisphere. Counting was conducted manually, except as described below, on 20 μm maximum projections of confocal section Z-stacks. DAPI staining was used to identify individual cells and to aid cell counting. For *in situ* studies, 60-80 12 μm sections were collected per hippocampal injection and 40-60 12 μm sections were collected per cortical injection. Non-consecutive sections were imaged to avoid double-counting cells that may have spanned neighboring sections and to sample more of the injected area. Z-stacks were not collected for *in situ* images. In the cortex, all cells were counted, and values are reported based on the total cell number. In the hippocampus, high cell densities precluded counting all cells; instead, all fluorescent cells were counted. Occasionally, sectioning removed the nucleus of a labeled cell, eliminating the DAPI signal; if signal was unambiguous, the cell was counted. Most counts were performed manually.

Two sets of analyses were done for each cell targeting experiment. Promoter specificity was calculated as the percentage of virus-labeled cells that were positive for the intrinsic marker M, such as SST or PV (XFP^+M^+/XFP^+). Coverage was the percentage of cells expressing an intrinsic marker M that had been labeled by the virus within the injection site (XFP^+M^+/M^+). For each promoter, brain region and species, 3-8 non-consecutive sections were counted and mean ± SE (standard error of the mean) was calculated. Data were collected from 2-4 mice and gerbils for each promoter and brain region; data were also collected from four marmosets to demonstrate promoter specificity (experiment-specific numbers of animals, sections and cells counted to generate the reported coverage and specificity are detailed in figure legends).

To quantify weak versus strong reporter expression from the h12R and h56D promoters, five sections from two mice per promoter were analyzed using ImageJ to estimate mean fluorescence intensities. *In situ* images with maximum coverage of the hippocampus (excluding the dentate gyrus) were selected for both h12R and h56D 10-11 days post-injection. A threshold was selected manually across all images to ensure the maximum dynamic range for covering both weakly and strongly labeled cells. The particle analysis tool in ImageJ was then used to determine the cell mean fluorescence intensity (in abstract units). The histogram of mean fluorescence intensities from the h12R promoter was significantly bimodal (Hartigan's Dip Statistic $p < 0.002$; Hartigan and Hartigan, 1985) and the modes were clearly segregated by a threshold. Given the bimodal distribution of the h12R intensities, we segregated the two modes using a threshold placed at 2000, a location marking a nadir between the modes, which were centered at 1483 and 2763. Cells exhibiting less than 2000 units mean fluorescence were considered weakly expressing.

Supplementary Material

Refer to Web version on PubMed Central for supplementary material.

ACKNOWLEDGMENTS

We thank Stefanie Esmond, Madeleine H. Flexer Harrison, Miles Morgan, Devon Greer, Shruti Patil, and Amanda Heatherly for technical assistance. This work was supported by NIH BRAIN Initiative grants U01NS094330 to N.J.P. and B.V.Z., U01NS099720 to E.S. and B.V.Z., and U19NS104590 to A.L.

REFERENCES

Adesnik H, Bruns W, Taniguchi H, Huang ZJ, and Scanziani M (2012). A neural circuit for spatial summation in visual cortex. Nature 490, 226–231. [PubMed: 23060193]

Allen K, Fuchs EC, Jaschonek H, Bannerman DM, and Monyer H (2011). Gap junctions between interneurons are required for normal spatial coding in the hippocampus and short-term spatial memory. J. Neurosci 31, 6542–6552. [PubMed: 21525295]

Armstrong C, Krook-Magnuson E, and Soltesz I (2012). Neurogliaform and ivy cells: a major family of nNOS expressing GABAergic neurons. Front. Neural Circuits 6, 23. [PubMed: 22623913]

Ascoli GA, Alonso-Nanclares L, Anderson SA, Barrionuevo G, Benavides-Piccione R, Burkhalter A, Buzsáki G, Cauli B, Defelipe J, Fairén A, et al.; Petilla Interneuron Nomenclature Group (2008). Petilla terminology: nomenclature of features of GABAergic interneurons of the cerebral cortex. Nat. Rev. Neurosci 9, 557–568. [PubMed: 18568015]

Aurnhammer C, Haase M, Muether N, Hausl M, Rauschhuber C, Huber I, Nitschko H, Busch U, Sing A, Ehrhardt A, and Baiker A (2012). Universal real-time PCR for the detection and quantification of

adeno-associated virus serotype 2-derived inverted terminal repeat sequences. Hum. Gene Ther. Methods 23, 18–28. [PubMed: 22428977]

Baraban SC, Hollopeter G, Erickson JC, Schwartzkroin PA, and Palmiter RD (1997). Knock-out mice reveal a critical antiepileptic role for neuropeptide Y. J. Neurosci 17, 8927–8936. [PubMed: 9364040]

Beck CF, Mutzel R, Barbé J, and Müller W (1982). A multifunctional gene (tetR) controls Tn10-encoded tetracycline resistance. J. Bacteriol 150, 633–642. [PubMed: 6279565]

Benson DL, Isackson PJ, Hendry SH, and Jones EG (1991). Differential gene expression for glutamic acid decarboxylase and type II calcium-calmodulin-dependent protein kinase in basal ganglia, thalamus, and hypothalamus of the monkey. J. Neurosci 11, 1540–1564. [PubMed: 1646294]

Benson DL, Isackson PJ, Gall CM, and Jones EG (1992). Contrasting patterns in the localization of glutamic acid decarboxylase and Ca2+/calmodulin protein kinase gene expression in the rat central nervous system. Neuroscience 46, 825–849. [PubMed: 1311814]

Betley JN, and Sternson SM (2011). Adeno-associated viral vectors for mapping, monitoring, and manipulating neural circuits. Hum. Gene Ther 22, 669–677. [PubMed: 21319997]

Borghuis BG, Tian L, Xu Y, Nikonov SS, Vardi N, Zemelman BV, and Looger LL (2011). Imaging light responses of targeted neuron populations in the rodent retina. J. Neurosci 31, 2855–2867. [PubMed: 21414907]

Bray NL, Pimentel H, Melsted P, and Pachter L (2016). Near-optimal probabilistic RNA-seq quantification. Nat. Biotechnol 34, 525–527. [PubMed: 27043002]

Bulfone A, Puelles L, Porteus MH, Frohman MA, Martin GR, and Rubenstein JL (1993). Spatially restricted expression of Dlx-1, Dlx-2 (Tes-1), Gbx-2, and Wnt-3 in the embryonic day 12.5 mouse forebrain defines potential transverse and longitudinal segmental boundaries. J. Neurosci 13, 3155–3172. [PubMed: 7687285]

Caputi A, Melzer S, Michael M, and Monyer H (2013). The long and short of GABAergic neurons. Curr. Opin. Neurobiol 23, 179–186. [PubMed: 23394773]

Cembrowski MS, and Menon V (2018). Continuous variation within cell types of the nervous system. Trends Neurosci 41, 337–348. [PubMed: 29576429]

Cembrowski MS, Bachman JL, Wang L, Sugino K, Shields BC, and Spruston N (2016). Spatial gene-expression gradients underlie prominent heterogeneity of CA1 pyramidal neurons. Neuron 89, 351–368. [PubMed: 26777276]

Chiu CQ, Lur G, Morse TM, Carnevale NT, Ellis-Davies GCR, and Higley MJ (2013). Compartmentalization of GABAergic inhibition by dendritic spines. Science 340, 759–762. [PubMed: 23661763]

Cobb SR, Buhl EH, Halasy K, Paulsen O, and Somogyi P (1995). Synchronization of neuronal activity in hippocampus by individual GABAergic interneurons. Nature 378, 75–78. [PubMed: 7477292]

Cobos I, Calcagnotto ME, Vilaythong AJ, Thwin MT, Noebels JL, Baraban SC, and Rubenstein JLR (2005). Mice lacking Dlx1 show subtype-specific loss of interneurons, reduced inhibition and epilepsy. Nat. Neurosci 8, 1059–1068. [PubMed: 16007083]

Cobos I, Borello U, and Rubenstein JLR (2007). Dlx transcription factors promote migration through repression of axon and dendrite growth. Neuron 54, 873–888. [PubMed: 17582329]

Decressac M, and Barker RA (2012). Neuropeptide Y and its role in CNS disease and repair. Exp. Neurol 238, 265–272. [PubMed: 23022456]

Dimidschstein J, Chen Q, Tremblay R, Rogers SL, Saldi G-A, Guo L, Xu Q, Liu R, Lu C, Chu J, et al. (2016). A viral strategy for targeting and manipulating interneurons across vertebrate species. Nat. Neurosci 19, 1743–1749. [PubMed: 27798629]

Dittgen T, Nimmerjahn A, Komai S, Licznerski P, Waters J, Margrie TW, Helmchen F, Denk W, Brecht M, and Osten P (2004). Lentivirus-based genetic manipulations of cortical neurons and their optical and electrophysiological monitoring in vivo. Proc. Natl. Acad. Sci. U S A 101, 18206–18211. [PubMed: 15608064]

El-Shamayleh Y, Kojima Y, Soetedjo R, and Horwitz GD (2017). Selective optogenetic control of Purkinje cells in monkey cerebellum. Neuron 95, 51–62.e4. [PubMed: 28648497]

Ellies DL, Stock DW, Hatch G, Giroux G, Weiss KM, and Ekker M (1997). Relationship between the genomic organization and the overlapping embryonic expression patterns of the zebrafish dlx genes. Genomics 45, 580–590. [PubMed: 9367683]

Földy C, Darmanis S, Aoto J, Malenka RC, Quake SR, and Südhof TC (2016). Single-cell RNAseq reveals cell adhesion molecule profiles in electrophysiologically defined neurons. Proc. Natl. Acad. Sci. U S A 113, E5222–E5231. [PubMed: 27531958]

Freund TF, and Buzsáki G (1996). Interneurons of the hippocampus. Hippocampus 6, 347–470. [PubMed: 8915675]

Fuchs EC, Zivkovic AR, Cunningham MO, Middleton S, Lebeau FEN, Bannerman DM, Rozov A, Whittington MA, Traub RD, Rawlins JNP, and Monyer H (2007). Recruitment of parvalbumin-positive interneurons determines hippocampal function and associated behavior. Neuron 53,591–604. [PubMed: 17296559]

Fuentealba P, Begum R, Capogna M, Jinno S, Márton LF, Csicsvari J, Thomson A, Somogyi P, and Klausberger T (2008). Ivy cells: a population of nitric-oxide-producing, slow-spiking GABAergic neurons and their involvement in hippocampal network activity. Neuron 57, 917–929. [PubMed: 18367092]

Gelman DM, Martini FJ, Nóbrega-Pereira S, Pierani A, Kessaris N, and Marín O (2009). The embryonic preoptic area is a novel source of cortical GABAergic interneurons. J. Neurosci 29, 9380–9389. [PubMed: 19625528]

Ghanem N, Jarinova O, Amores A, Long Q, Hatch G, Park BK, Rubenstein JLR, and Ekker M (2003). Regulatory roles of conserved intergenic domains in vertebrate Dlx bigene clusters. Genome Res 13, 533–543. [PubMed: 12670995]

Gossen M, and Bujard H (1992). Tight control of gene expression in mammalian cells by tetracycline-responsive promoters. Proc. Natl. Acad. Sci. U S A 89, 5547–5551. [PubMed: 1319065]

Gossen M, Freundlieb S, Bender G, Müller G, Hillen W, and Bujard H (1995). Transcriptional activation by tetracyclines in mammalian cells. Science 268, 1766–1769. [PubMed: 7792603]

Grieger JC, Choi VW, and Samulski RJ (2006). Production and characterization of adeno-associated viral vectors. Nat. Protoc 1, 1412–1428. [PubMed: 17406430]

Guizar-Sicairos M, Thurman ST, and Fienup JR (2008). Efficient subpixel image registration algorithms. Opt. Lett 33, 156–158. [PubMed: 18197224]

Han X, Qian X, Bernstein JG, Zhou H-H, Franzesi GT, Stern P, Bronson RT, Graybiel AM, Desimone R, and Boyden ES (2009). Millisecond-timescale optical control of neural dynamics in the nonhuman primate brain. Neuron 62, 191–198. [PubMed: 19409264]

Harris KD, Gonzales CB, Hochgerner H, Skene NG, Magno L, Katona L, Somogyi P, Kessaris N, Linnarsson S, and Hjerling-Leffler J (2017). Classes and continua of hippocampal CA1 inhibitory neurons revealed by single-cell transcriptomics. bioRxiv. 10.1101/143354.

Hartigan JA, and Hartigan PM (1985). The dip test of unimodality. Ann. Stat 13, 70–84.

He M, Tucciarone J, Lee S, Nigro MJ, Kim Y, Levine JM, Kelly SM, Krugikov I, Wu P, Chen Y, et al. (2016). Strategies and tools for combinatorial targeting of GABAergic neurons in mouse cerebral cortex. Neuron 91, 1228–1243. [PubMed: 27618674]

Hillen W, and Berens C (1994). Mechanisms underlying expression of Tn10 encoded tetracycline resistance. Annu. Rev. Microbiol 48, 345–369. [PubMed: 7826010]

Hu H, Gan J, and Jonas P (2014). Interneurons. Fast-spiking, parvalbumin^{+} GABAergic interneurons: from cellular design to microcircuit function. Science 345,1255263. [PubMed: 25082707]

Huang X, Elyada YM, Bosking WH, Walker T, and Fitzpatrick D (2014). Optogenetic assessment of horizontal interactions in primary visual cortex. J. Neurosci 34, 4976–4990. [PubMed: 24695715]

Jia H, Rochefort NL, Chen X, and Konnerth A (2011). In vivo two-photon imaging of sensory-evoked dendritic calcium signals in cortical neurons. Nat. Protoc 6, 28–35. [PubMed: 21212780]

Jinno S, and Kosaka T (2004). Patterns of colocalization of neuronal nitric oxide synthase and somatostatin-like immunoreactivity in the mouse hippocampus: quantitative analysis with optical disector. Neuroscience 124, 797–808. [PubMed: 15026120]

Jinno S, and Kosaka T (2006). Cellular architecture of the mouse hippocampus: a quantitative aspect of chemically defined GABAergic neurons with stereology. Neurosci. Res 56, 229–245. [PubMed: 16930755]

Kaifosh P, Lovett-Barron M, Turi GF, Reardon TR, and Losonczy A (2013). Septo-hippocampal GABAergic signaling across multiple modalities in awake mice. Nat. Neurosci 16, 1182–1184. [PubMed: 23912949]

Kaifosh P, Zaremba JD, Danielson NB, and Losonczy A (2014). SIMA: Python software for analysis of dynamic fluorescence imaging data. Front. Neuroinform 8, 80. [PubMed: 25295002]

Khan A, Fornes O, Stigliani A, Gheorghe M, Castro-Mondragon JA, van der Lee R, Bessy A, Chfbneby J, Kulkarni SR, Tan G, et al. (2018). JASPAR 2018: update of the open-access database of transcription factor binding profiles and its web framework. Nucleic Acids Res 46 (D1), D260–D266. [PubMed: 29140473]

Klausberger T, and Somogyi P (2008). Neuronal diversity and temporal dynamics: the unity of hippocampal circuit operations. Science 321, 53–57. [PubMed: 18599766]

Kranz A, Fu J, Duerschke K, Weidlich S, Naumann R, Stewart AF, and Anastassiadis K (2010). An improved Flp deleter mouse in C57Bl/6 based on Flpo recombinase. Genesis 48, 512–520. [PubMed: 20506501]

Lahti L, Achim K, and Partanen J (2013). Molecular regulation of GABAergic neuron differentiation and diversity in the developing midbrain. Acta Physiol. (Oxf.) 207, 616–627. [PubMed: 23297792]

Lee S, Kruglikov I, Huang ZJ, Fishell G, and Rudy B (2013). A disinhibitory circuit mediates motor integration in the somatosensory cortex. Nat. Neurosci 16, 1662–1670. [PubMed: 24097044]

Lee AT, Vogt D, Rubenstein JL, and Sohal VS (2014). A class of GABAergic neurons in the prefrontal cortex sends long-range projections to the nucleus accumbens and elicits acute avoidance behavior. J. Neurosci 34, 11519–11525. [PubMed: 25164650]

Lein ES, Hawrylycz MJ, Ao N, Ayres M, Bensinger A, Bernard A, Boe AF, Boguski MS, Brockway KS, Byrnes EJ, et al. (2007). Genome-wide atlas of gene expression in the adult mouse brain. Nature 445, 168–176. [PubMed: 17151600]

Lewis DA, Hashimoto T, and Volk DW (2005). Cortical inhibitory neurons and schizophrenia. Nat. Rev. Neurosci 6, 312–324. [PubMed: 15803162]

Long JE, Cobos I, Potter GB, and Rubenstein JLR (2009). Dlx1&2 and Mash1 transcription factors control MGE and CGE patterning and differentiation through parallel and overlapping pathways. Cereb. Cortex 19 (Suppl 1), i96–i106. [PubMed: 19386638]

Lovett-Barron M, Turi GF, Kaifosh P, Lee PH, Bolze F, Sun X-H, Nicoud J-F, Zemelman BV, Sternson SM, and Losonczy A (2012). Regulation of neuronal input transformations by tunable dendritic inhibition. Nat. Neurosci 15, 423–430. [PubMed: 22246433]

Lovett-Barron M, Kaifosh P, Kheirbek MA, Danielson N, Zaremba JD, Reardon TR, Turi GF, Hen R, Zemelman BV, and Losonczy A (2014). Dendritic inhibition in the hippocampus supports fear learning. Science 343, 857–863. [PubMed: 24558155]

Madisen L, Zwingman TA, Sunkin SM, Oh SW, Zariwala HA, Gu H, Ng LL, Palmiter RD, Hawrylycz MJ, Jones AR, et al. (2010). A robust and high-throughput Cre reporting and characterization system for the whole mouse brain. Nat. Neurosci 13, 133–140. [PubMed: 20023653]

Meyer HS, Schwarz D, Wimmer VC, Schmitt AC, Kerr JND, Sakmann B, and Helmstaedter M (2011). Inhibitory interneurons in a cortical column form hot zones of inhibition in layers 2 and 5A. Proc. Natl. Acad. Sci. U S A 108, 16807–16812. [PubMed: 21949377]

Milstein AD, Bloss EB, Apostolides PF, Vaidya SP, Dilly GA, Zemelman BV, and Magee JC (2015). Inhibitory gating of input comparison in the CA1 microcircuit. Neuron 87, 1274–1289. [PubMed: 26402609]

Mitchell JF, Priebe NJ, and Miller CT (2015). Motion dependence of smooth pursuit eye movements in the marmoset. J. Neurophysiol 113, 3954–3960. [PubMed: 25867740]

Miyoshi G, and Fishell G (2011). GABAergic interneuron lineages selectively sort into specific cortical layers during early postnatal development. Cereb. Cortex 21, 845–852. [PubMed: 20732898]

Mo A, Mukamel EA, Davis FP, Luo C, Henry GL, Picard S, Urich MA, Nery JR, Sejnowski TJ, Lister R, et al. (2015). Epigenomic signatures of neuronal diversity in the mammalian brain. Neuron 86, 1369–1384. [PubMed: 26087164]

Muñoz W, Tremblay R, Levenstein D, and Rudy B (2017). Layer-specific modulation of neocortical dendritic inhibition during active wakefulness. Science 355, 954–959. [PubMed: 28254942]

Murray SA, Eppig JT, Smedley D, Simpson EM, and Rosenthal N (2012). Beyond knockouts: cre resources for conditional mutagenesis. Mamm. Genome 23, 587–599. [PubMed: 22926223]

Nathanson JL, Yanagawa Y, Obata K, and Callaway EM (2009a). Preferential labeling of inhibitory and excitatory cortical neurons by endogenous tropism of adeno-associated virus and lentivirus vectors. Neuroscience 161, 441–450. [PubMed: 19318117]

Nathanson JL, Jappelli R, Scheeff ED, Manning G, Obata K, Brenner S, and Callaway EM (2009b). Short promoters in viral vectors drive selective expression in mammalian inhibitory neurons, but do not restrict activity to specific inhibitory cell-types. Front. Neural Circuits 3, 19. [PubMed: 19949461]

Noè F, Pool A-H, Nissinen J, Gobbi M, Bland R, Rizzi M, Balducci C, Ferraguti F, Sperk G, During MJ, et al. (2008). Neuropeptide Y gene therapy decreases chronic spontaneous seizures in a rat model of temporal lobe epilepsy. Brain 131, 1506–1515. [PubMed: 18477594]

Ovcharenko I, Nobrega MA, Loots GG, and Stubbs L (2004). ECR Browser: a tool for visualizing and accessing data from comparisons of multiple vertebrate genomes. Nucleic Acids Res 32, W280–W286. [PubMed: 15215395]

Paul A, Crow M, Raudales R, He M, Gillis J, and Huang ZJ (2017). Transcriptional architecture of synaptic communication delineates GABAergic neuron identity. Cell 171, 522–539.e20. [PubMed: 28942923]

Pfeffer CK, Xue M, He M, Huang ZJ, and Scanziani M (2013). Inhibition of inhibition in visual cortex: the logic of connections between molecularly distinct interneurons. Nat. Neurosci 16, 1068–1076. [PubMed: 23817549]

Potter GB, Petryniak MA, Shevchenko E, McKinsey GL, Ekker M, and Rubenstein JLR (2009). Generation of Cre-transgenic mice using Dlx1/Dlx2 enhancers and their characterization in GABAergic interneurons. Mol. Cell. Neurosci 40, 167–186. [PubMed: 19026749]

Raymond CS, and Soriano P (2007). High-efficiency FLP and PhiC31 site-specific recombination in mammalian cells. PLoS ONE 2, e162. [PubMed: 17225864]

Royer S, Zemelman BV, Losonczy A, Kim J, Chance F, Magee JC, and Buzsáki G (2012). Control of timing, rate and bursts of hippocampal place cells by dendritic and somatic inhibition. Nat. Neurosci 15, 769–775. [PubMed: 22446878]

Rudy B, Fishell G, Lee S, and Hjerling-Leffler J (2011). Three groups of interneurons account for nearly 100% of neocortical GABAergic neurons. Dev. Neurobiol 71, 45–61. [PubMed: 21154909]

Samulski RJ, Chang LS, and Shenk T (1989). Helper-free stocks of recombinant adeno-associated viruses: normal integration does not require viral gene expression. J. Virol 83, 3822–3828.

Schlake T, and Bode J (1994). Use of mutated FLP recognition target (FRT) sites for the exchange of expression cassettes at defined chromosomal loci. Biochemistry 33, 12746–12751. [PubMed: 7947678]

Schoch S, Cibelli G, and Thiel G (1996). Neuron-specific gene expression of synapsin I. Major role of a negative regulatory mechanism. J. Biol. Chem 271, 3317–3323. [PubMed: 8621737]

Schoenenberger P, O'Neill J, and Csicsvari J (2016). Activity-dependent plasticity of hippocampal place maps. Nat. Commun 7, 11824. [PubMed: 27282121]

Scholl B, Pattadkal JJ, Dilly GA, Priebe NJ, and Zemelman BV (2015). Local integration accounts for weak selectivity of mouse neocortical parvalbumin interneurons. Neuron 87, 424–436. [PubMed: 26182423]

Scholl B, Pattadkal JJ, Rowe A, and Priebe NJ (2017). Functional characterization and spatial clustering of visual cortical neurons in the predatory grasshopper mouse *Onychomys arenicola*. J. Neurophysiol 117, 910–918. [PubMed: 27927787]

Seibler J, and Bode J (1997). Double-reciprocal crossover mediated by FLP-recombinase: a concept and an assay. Biochemistry 36, 1740–1747. [PubMed: 9048557]

Seidemann E, Chen Y, Bai Y, Chen SC, Mehta P, Kajs BL, Geisler WS, and Zemelman BV (2016). Calcium imaging with genetically encoded indicators in behaving primates. eLife 5, 3771.

Shimshek DR, Kim J, Hübner MR, Spergel DJ, Buchholz F, Casanova E, Stewart AF, Seeburg PH, and Sprengel R (2002). Codon-improved Cre recombinase (iCre) expression in the mouse. Genesis 32, 19–26. [PubMed: 11835670]

Simon A, Oláh S, Molnár G, Szabadics J, and Tamás G (2005). Gap-junctional coupling between neurogliaform cells and various interneuron types in the neocortex. J. Neurosci 25, 6278–6285. [PubMed: 16000617]

Soltesz I, and Losonczy A (2018). CA1 pyramidal cell diversity enabling parallel information processing in the hippocampus. Nat. Neurosci 21, 484–493. [PubMed: 29593317]

Stauffer WR, Lak A, Yang A, Borel M, Paulsen O, Boyden ES, and Schultz W (2016). Dopamine neuron-specific optogenetic stimulation in rhesus macaques. Cell 166, 1564–1571.e6. [PubMed: 27610576]

Stühmer T, Anderson SA, Ekker M, and Rubenstein JLR (2002a). Ectopic expression of the Dlx genes induces glutamic acid decarboxylase and Dlx expression. Development 129, 245–252. [PubMed: 11782417]

Stühmer T, Puelles L, Ekker M, and Rubenstein JLR (2002b). Expression from a Dlx gene enhancer marks adult mouse cortical GABAergic neurons. Cereb. Cortex 12, 75–85. [PubMed: 11734534]

Sumiyama K, Irvine SQ, Stock DW, Weiss KM, Kawasaki K, Shimizu N, Shashikant CS, Miller W, and Ruddle FH (2002). Genomic structure and functional control of the Dlx3–7 bigene cluster. Proc. Natl. Acad. Sci. U S A 99, 780–785. [PubMed: 11792834]

Tang YT, Hu T, Arterburn M, Boyle B, Bright JM, Emtage PC, and Funk WD (2005). PAQR proteins: a novel membrane receptor family defined by an ancient 7-transmembrane pass motif. J. Mol. Evol 61, 372–380. [PubMed: 16044242]

Taniguchi H, He M, Wu P, Kim S, Paik R, Sugino K, Kvitsiani D, Fu Y, Lu J, Lin Y, et al. (2011). A resource of Cre driver lines for genetic targeting of GABAergic neurons in cerebral cortex. Neuron 71, 995–1013. [PubMed: 21943598]

Tasic B, Menon V, Nguyen TN, Kim TK, Jarsky T, Yao Z, Levi B, Gray LT, Sorensen SA, Dolbeare T, et al. (2016). Adult mouse cortical cell taxonomy revealed by single cell transcriptomics. Nat. Neurosci 19, 335–346. [PubMed: 26727548]

Tenenbaum L, Chtarto A, Lehtonen E, Velu T, Brotchi J, and Levivier M (2004). Recombinant AAV-mediated gene delivery to the central nervous system. J. Gene Med 6 (Suppl 1), S212–S222. [PubMed: 14978764]

Thompson CL, Pathak SD, Jeromin A, Ng LL, MacPherson CR, Mortrud MT, Cusick A, Riley ZL, Sunkin SM, Bernard A, et al. (2008). Genomic anatomy of the hippocampus. Neuron 60, 1010–1021. [PubMed: 19109908]

Tricoire L, and Vitalis T (2012). Neuronal nitric oxide synthase expressing neurons: a journey from birth to neuronal circuits. Front. Neural Circuits 6, 82. [PubMed: 23227003]

van den Pol AN, Yao Y, Fu L-Y, Foo K, Huang H, Coppari R, Lowell BB, and Broberger C (2009). Neuromedin B and gastrin-releasing peptide excite arcuate nucleus neuropeptide Y neurons in a novel transgenic mouse expressing strong Renilla green fluorescent protein in NPY neurons. J. Neurosci 29, 4622–4639. [PubMed: 19357287]

Wang X, Zhang C, Szabo G, and Sun Q-Q (2013). Distribution of CaMKIIα expression in the brain in vivo, studied by CaMKIIα-GFP mice. Brain Res 1518, 9–25. [PubMed: 23632380]

Watakabe A, Ohtsuka M, Kinoshita M, Takaji M, Isa K, Mizukami H, Ozawa K, Isa T, and Yamamori T (2015). Comparative analyses of adeno-associated viral vector serotypes 1, 2, 5, 8 and 9 in marmoset, mouse and macaque cerebral cortex. Neurosci. Res 93, 144–157. [PubMed: 25240284]

Wylie DC, Hofmann HA, and Zemelman BV (2018). SArKS: discovering gene expression regulatory motifs and domains by suffix array kernel smoothing. bioRxiv. 10.1101/133934.

Xu H, Jeong H-Y, Tremblay R, and Rudy B (2013). Neocortical somato-statin-expressing GABAergic interneurons disinhibit the thalamorecipient layer4. Neuron 77, 155–167. [PubMed: 23312523]

Yao F, Svensjö T, Winkler T, Lu M, Eriksson C, and Eriksson E (1998). Tetracycline repressor, tetR, rather than the tetR-mammalian cell transcription factor fusion derivatives, regulates inducible gene expression in mammalian cells. Hum. Gene Ther 9, 1939–1950. [PubMed: 9741432]

Zeisel A, Muñoz-Manchado AB, Codeluppi S, Lönnerberg P, La Manno G, Juréus A, Marques S, Munguba H, He L, Betsholtz C, et al. (2015). Brain structure. Cell types in the mouse cortex and hippocampus revealed by single-cell RNA-seq. Science 347, 1138–1142. [PubMed: 25700174]

Zerucha T, Stühmer T, Hatch G, Park BK, Long Q, Yu G, Gambarotta A, Schultz JR, Rubenstein JL, and Ekker M (2000). A highly conserved enhancer in the Dlx5/Dlx6 intergenic region is the site of cross-regulatory interactions between Dlx genes in the embryonic forebrain. J. Neurosci 20, 709–721. [PubMed: 10632600]

Highlights

- Conserved genomic elements allow access to primate and rodent neuron subclasses
- Single viral constructs provide broad access to forebrain GABAergic neurons
- Interdependent constructs restrict access to PV^+, SST^+, and NPY^+ neuron subclasses
- Methods allow interrogations of cortical circuit elements in non-transgenic animals

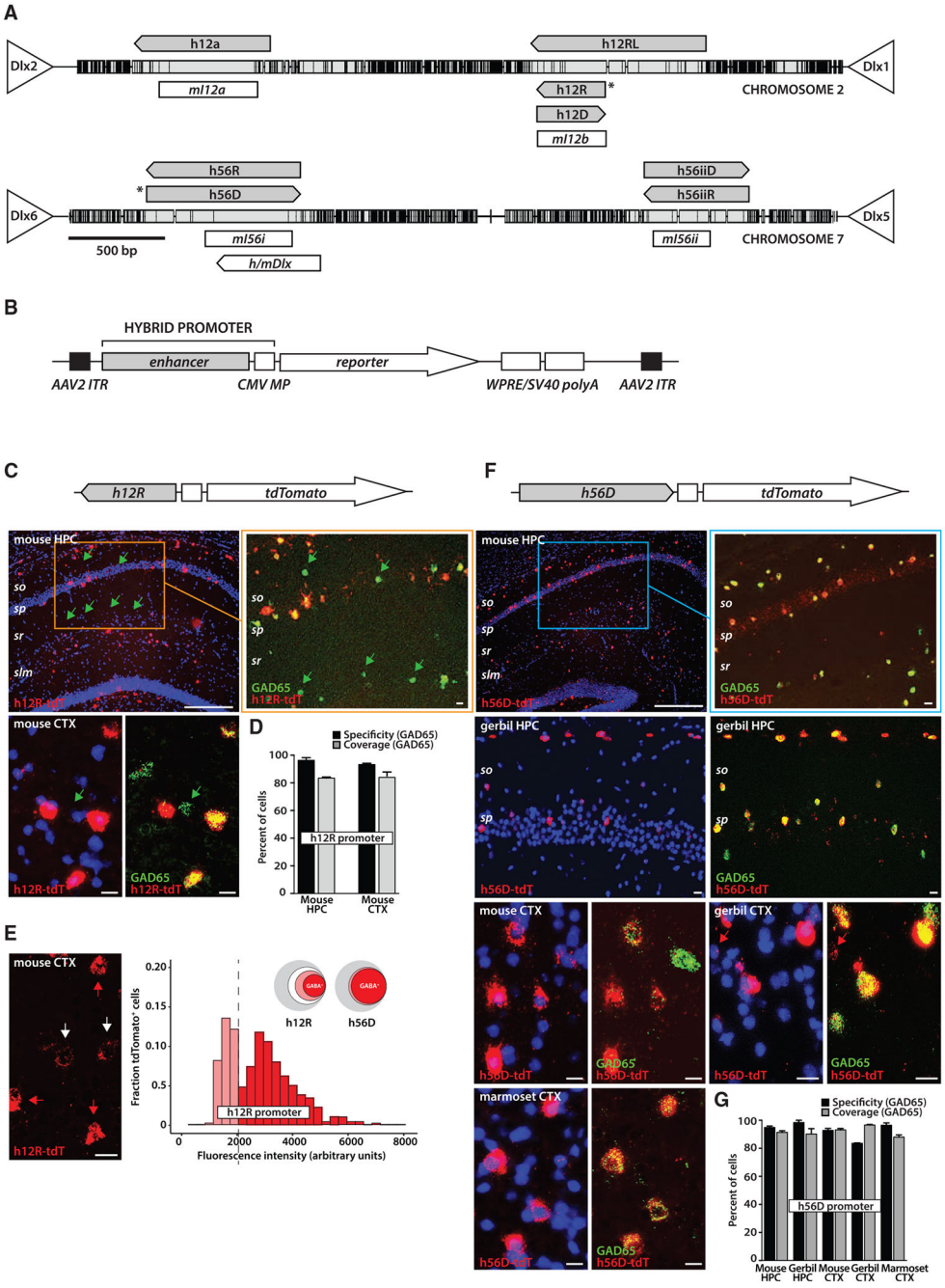

Figure 1. Organization and Specificity of Candidate GABAergic Promoters

(A) Human *Dlx1/2* and *Dlx5/6* intergenic regions were aligned *de novo* to mouse genomic DNA. Human genomic segments are shown, black lines depict base pair differences; tested enhancers are in gray, those selected for targeting studies are marked by asterisks. Enhancers described previously (Dittgen et al., 2004; Ghanem et al., 2003; Dimidschstein et al., 2016) are in white. Where applicable, arrowheads indicate the original orientations of the cloned enhancer domains within chromosomal DNA. Scale bar, 500 base pairs (bp).

(B) A typical rAAV construct comprised a hybrid promoter consisting of an enhancer domain from (A), the cytomegalovirus minimal promoter (CMV MP), a reporter protein coding sequence, woodchuck hepatitis virus posttranscriptional regulatory element (WPRE), and simian virus 40 polyadenylation sequence, all flanked by AAV2 inverted terminal repeats (ITRs).

(C) The rAAV vector h12R-tdTomato was injected into mouse hippocampal area CA1 (top) and cortex (bottom). Brain sections were analyzed by *in situ* mRNA hybridization using probes to tdTomato (tdT; red) and to endogenous glutamic acid decarboxylase (GAD65; green) transcripts (insets). Green arrows mark GABAergic cells not labeled by the virus. h12R promoter was mostly inactive in strata radiatum and lacunosum-moleculare neurons. Subsequent analysis indicated that many of the missed cells were NPY^+ and VIP^+ (see Figure 3).

(D) Targeting quantitation, indicated as mean ± SE. Mouse HPC: specificity 96.3% ± 1.9%, coverage 83.4% ± 0.8% (n = 4 sections, 4 mice, 262 $GAD65^+$ cells); mouse CTX: specificity 92.8% ± 2.0%, coverage 84.0% ± 2.8% (n = 4 sections, 2 mice, 1,418 cells).

(E) Cortical panel shows examples of high and low reporter expression from the h12R promoter (weak expression, 177; strong expression, 328; 35%; n = 5 sections, 2 mice, 505 tdT^+ cells). Histogram shows the bimodal distribution ($p < 0.002$, Hartigan's dip statistic) of reporter expression estimated using cell mean fluorescence intensity as described in Method Details in the STAR Methods. Bin width was 300 fluorescence units; cells below 2,000 units intensity were considered weakly expressing. Schematics depict relative expression from each GABAergic promoter: strong expression (red), weak expression (pink), no expression (white), and non-GABAergic cells (gray).

(F) The rAAV vector h56D-tdTomato was injected into mouse and gerbil hippocampal area CA1 (top and middle) and mouse, gerbil, and marmoset cortex (bottom). Brain sections were analyzed as in (C). Red arrow points to a gerbil virus-targeted cell that was not GABAergic; other cells were all GABAergic. Scale bars, 200 μm for panel 1, 20 μm for all other panels, including inset. so, stratum oriens; sp, stratum pyramidale; sr, stratum radiatum; slm, stratum lacunosum-moleculare.

(G) Targeting quantitation, indicated as mean ± SE. Mouse HPC: specificity 94.9% ± 1.0%, coverage 91.4% ± 1.1% (n = 5 sections, 4 mice, 324 $GAD65^+$ cells); gerbil HPC: specificity 98.4% ± 1.6%, coverage 90.2% ± 4.0% (n = 3 sections, 2 gerbils, 85 $GAD65^+$ cells); mouse CTX: specificity 93.1% ± 1.0%, coverage 92.8% ± 1.4% (n = 5 sections, 2 mice, 1,256 cells); gerbil CTX: specificity 83.6% ± 0.3%, coverage 96.6% ± 0.4% (n = 3 sections, 2 gerbils, 769 cells); marmoset CTX: specificity 96.5% ± 1.6%, coverage 88.0% ± 1.5% (n = 3 sections, 1 animal, 1,569 cells). In all instances, specificity refers to the percentage tdT^+ (red) cells that are $GAD65^+$, reflecting the cell type specificity of the targeting vector; coverage is the percentage of GABAergic cells that had been labeled.

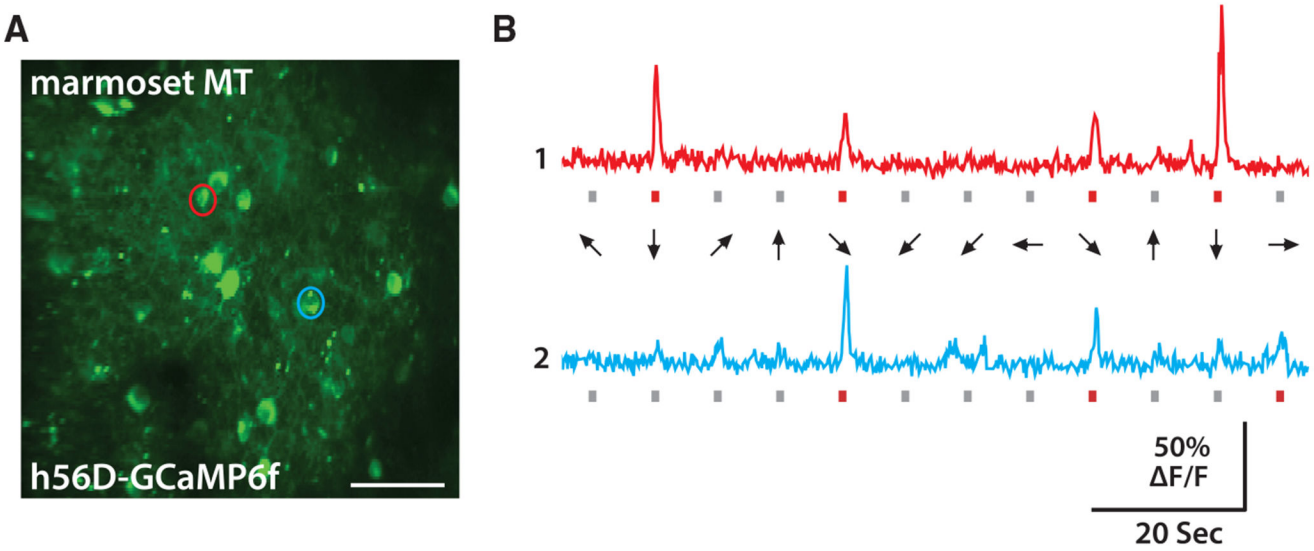

Figure 2. The h56D Promoter Supports Direct GCaMP6f Expression in Putative Inhibitory Neurons of Awake Behaving Primates

(A) Marmoset cortical area MT was injected with rAAV h56D-GCaMP6f. A representative imaging plane 8 weeks post-injection is shown. Scale bar, 50 μm.

(B) Responses to visual stimuli for two representative cells circled red and blue in (A) are shown. Bars below each trace mark stimulus presentations: red bars for the preferred stimulus, gray bars for the non-preferred stimulus. The motion direction for each stimulus is indicated by the arrows. Responses were first detected 6 weeks post-injection.

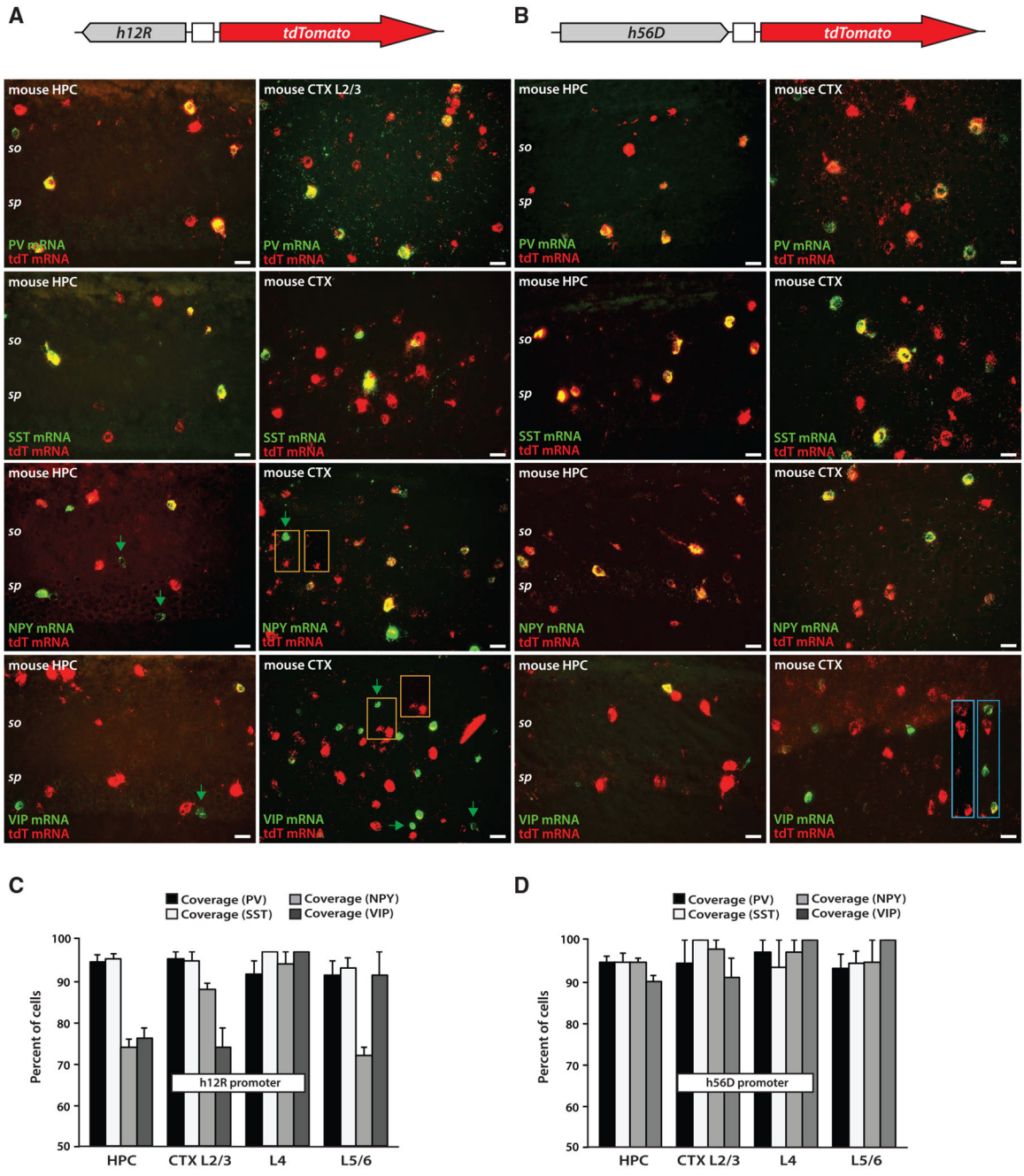

Figure 3. h12R and h56D Promoters Are Differentially Active in Subclasses of Mouse GABAergic Interneurons

(A and B) rAAV vectors h12R-tdTomato (A) and h56D-tdTomato (B) were injected into mouse hippocampal area CA1 (columns 1 and 3) and cortex (columns 2 and 4). Brain sections were analyzed by *in situ* mRNA hybridization using probes to tdTomato (tdT; red) and to each of PV, SST, NPY, and VIP (green) transcripts. All hippocampal and cortical layers were examined and counted, as in Figure 1, but only detailed images are shown. (A) First column: the h12R promoter was active in nearly all hippocampal PV^+ and SST^+ interneurons but not in all NPY^+ and VIP^+ neurons. Second column: the h12R promoter was

active in nearly all cortical PV^+ and SST^+ interneurons but inactive in some layer 2/3 and layer 5/6 NPY^+ and layer 2/3 VIP^+ neurons. Green arrows mark missed cells within each class. Orange-boxed insets (green channel omitted) show examples of NPY^+ and VIP^+ neurons that were not labeled by the virus (tdT^-).

(B) First column: the h56D promoter was active in nearly all neurons of each class. Second column: the h56D promoter was likewise active in nearly all cortical neurons of each class. Blue-boxed inset (green channel omitted) shows that even seemingly green-only VIP^+ neurons were tdT^+. Scale bars, 20 μm throughout. so, stratum oriens; sp, stratum pyramidale.

(C) Targeting quantitation (coverage) for h12R, indicated as mean ± SE, by class and cortical layer. Mouse HPC (n = 5 sections, 3 mice per probe): PV 97.2% ± 1.8% (69 PV^+ cells); SST 98.0% ± 1.4% (55 SST^+ cells); NPY 75.4% ± 2.0% (108 NPY^+ cells); VIP 77.7% ± 2.7% (24 VIP^+ cells). On the basis of these cell counts, the majority of neurons missed by h12R were NPY^+. Mouse CTX (n = 4 sections, 2 mice per probe): PV: L2/3 98.0% ± 2.0% (1,248 cells), L4 94.0% ± 3.6% (1,329 cells), L5/6 93.8% ± 3.8% (1,255 cells); SST: L2/3 97.5% ± 2.5% (1,132 cells), L4 100% ± 0% (1,376 cells), L5/6 95.7% ± 2.6% (1,285 cells); NPY: L2/3 90.3% ± 1.7% (1,339 cells), L4 96.8% ± 3.3% (1,200 cells), L5/6 73.3% ± 2.0% (1,261 cells); VIP: L2/3 75.3% ± 5.0% (966 cells), L4 100% ± 0% (1,353 cells) L5/6 93.8% ± 6.3% (1,212 cells).

(D) Targeting quantitation for h56D, indicated as mean ± SE, by class and cortical layer. Mouse HPC (n = 4 sections, 3 mice per probe): PV 94.5% ± 1.5% (78 PV^+ cells); SST94.6% ± 2.0% (62 SST^+ cells); NPY 94.5% ± 1.0% (99 NPY^+ cells); VIP 90.3% ± 1.7% (23 VIP^+ cells). Mouse CTX (n = 3 sections, 3 mice per probe): PV: L2/3 94.3% ± 5.7% (882 cells), L4 97.0% ± 3.0% (1,200 cells), L5/6 93.0% ± 3.5% (780 cells); SST: L2/3 100% ± 0% (796 cells), L4 93.3% ± 6.7% (671 cells), L5/6 94.3% ± 2.9% (802 cells); NPY: L2/3 97.6% ± 2.4% (791 cells), L4 97.0% ± 3.0% (1,148 cells), L5/6 94.4% ± 5.6% (831 cells); VIP: L2/3 90.8% ± 4.6% (850 cells), L4 100% ± 0% (855 cells), L5/6 100% ± 0% (780 cells).

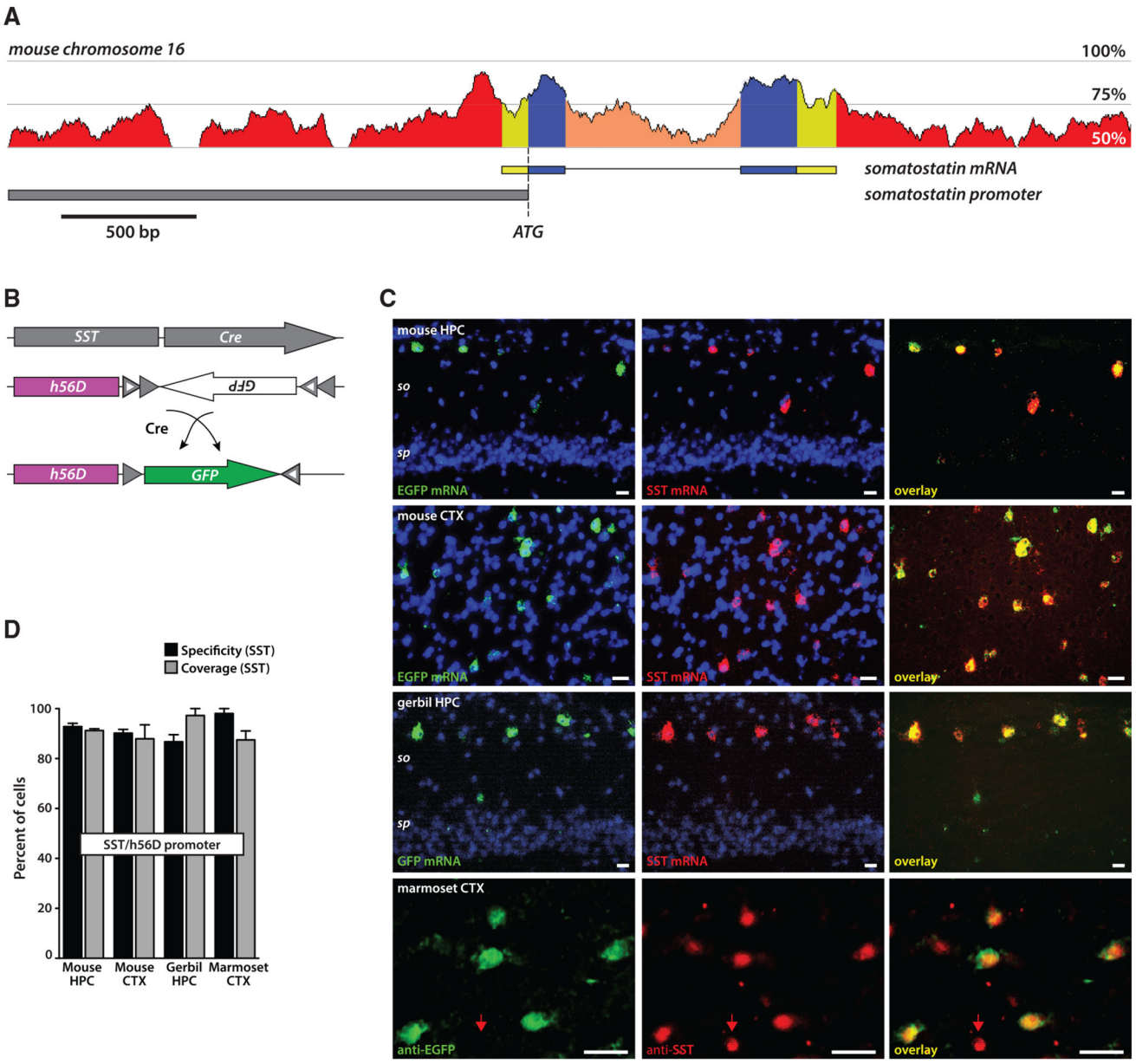

Figure 4. Set Intersection Strategy to Target Somatostatin Interneurons in Rodent and Primate

(A) Sequence conservation between mouse and human genomic DNA at the mouse *somatostatin* (SST) gene locus: UTRs (yellow), exons (blue), and intron (orange). Upstream and downstream non-coding regions (red) showed elevated sequence conservation, as indicated numerically at right. Selected promoter region extended ~2,000 bp upstream of the SST start codon, covering three conserved domains.

(B) Set intersection strategy: SST-Cre and h56D-(EGFP)^{Cre} viruses are co-injected; EGFP is expressed only when both promoters are active in the same cell.

(C) Representative hippocampal sections for mouse and gerbil and cortical layer 2/3 sections for mouse examined using *in situ* hybridization probes to EGFP (green) and SST (red) transcripts. Cell nuclei were additionally DAPI stained. Marmoset layer 2/3 cortical sections

were stained with antibodies against EGFP (green) and SST (red). Red arrow indicates an unlabeled SST^+ cell. Scale bars, 20 μm throughout. so, stratum oriens; sp, stratum pyramidale.

(D) Quantitation of SST^+ neuron targeting indicated as mean ± SE. Mouse HPC: specificity 92.3% ± 1.5%, coverage 91.3% ± 0.9% (n = 4 sections, 3 mice, 43 SST^+ cells). Mouse CTX: specificity 90.2% ± 1.5%, coverage 87.9% ± 5.6% (n = 3 sections, 2 mice, 769 cells). Gerbil HPC: specificity 86.7% ± 2.8%, coverage 97.2% ± 2.7% (n = 3 sections, 2 gerbils, 34 SST^+ cells) Marmoset CTX: specificity 98.5% ± 1.5%, coverage 88.3% ± 2.7% (n = 3 sections, 1 animal, 60 SST^+ cells).

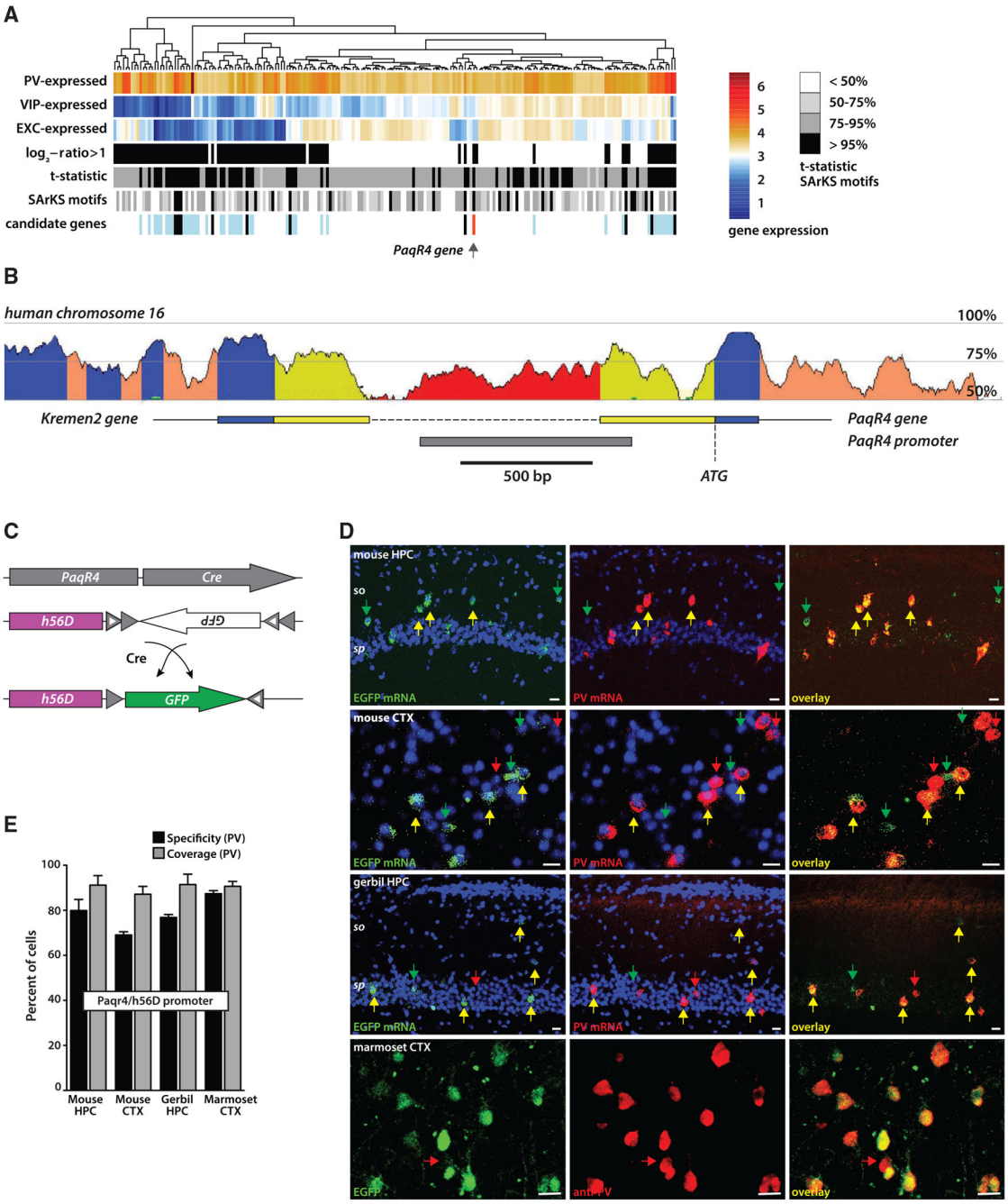

Figure 5. Set Intersection Strategy to Target Parvalbumin Interneurons in Rodent and Primate

(A) SArKS-facilitated selection ofthe *PaqR4* gene (Wylie et al., 2018). Cell class-specific transcriptome data (Mo et al., 2015) were hierarchically clustered on the basis of differential expression in PV^+, VIP^+, and excitatory (EXC) neurons (as shown in dendrogram). This set was further refined using (1)the $\log_2$ ratio of gene expression in PV^+ neurons compared with other neuron types (genes with values > 1 [black bars] were retained); (2) PV-versus-other differential expression *t*-statistic; and (3) SArKS motif-based regression model score. For (2) and (3), black bars mark the top 5% of the 6,326 SArKS-analyzed genes (see Method

Details in STAR Methods). The bottom row shows 11 genes that remain after all the filters have been applied (black bars) and genes that were eliminated by the SArKS filter (blue bars); PaqR4 (red bar) is indicated by an arrow.

(B) Sequence conservation between mouse and human genomic DNA at the human *PaqR4* gene locus is indicated numerically at right. *PaqR4* and the upstream *Kremen2* gene mRNA UTRs (yellow), exons (blue), and intron (orange) are shown. Selected non-coding region (red) extends ~800 bp upstream of the *PaqR4* transcription start site (TSS).

(C) Set intersection strategy: expression of EGFP occurs when PaqR4-Cre and h56D-$(EGFP)^{Cre}$ vectors are active in the same neuron.

(D) Hippocampal sections for mouse and gerbil and cortical layer 4 sections for mouse examined using *in situ* hybridization probes to EGFP (green) and PV (red) transcripts. Cell nuclei were additionally DAPI stained. Marmoset layer 4 cortical sections were stained with antibodies against EGFP (green) and SST (red). Scale bars, 20 μm throughout. Yellow arrows indicate $EGFP^+/PV^+$ double-positive cells, green arrows indicate $EGFP^+/PV^-$ cells, and red arrows point to $EGFP^-/PV^+$ cells. For clarity, not all $EGFP^+/PV^+$ cells are marked. Scale bars, 20 μm throughout. so, stratum oriens; sp, stratum pyramidale.

(E) Quantitation of PV^+ neuron targeting indicated as mean ± SE. Mouse HPC: specificity 79.8% ± 4.9%,coverage 91.3% ± 0.9% (n = 5 sections, 3 mice, 86 PV^+ cells). Gerbil HPC: specificity 76.8% ± 1.3%, coverage 91.4% ± 4.6% (n = 3 sections, 2 gerbils, 52 PV^+ cells). Mouse CTX: specificity 69.1% ± 1.4%, coverage 87.1% ± 3.5% (n = 3 sections, 2 mice, 813 cells). Marmoset CTX: specificity 87.4 ± 1.4, coverage: 87.1% ± 3.5% (n = 3 sections, 1 animal, 114 PV^+ cells).

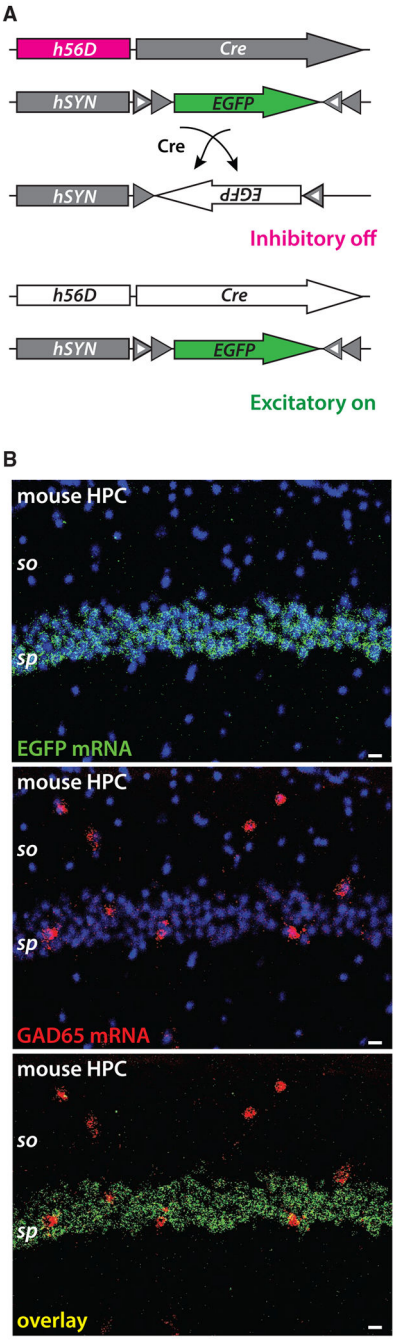

Figure 6. Set Difference Strategy to Target Mouse Hippocampal Excitatory Neurons

Hippocampal excitatory neurons were isolated using the h56D promoter to subtract GABAergic interneurons from all neurons.

(A) EGFP is *floxed* in the forward orientation, such that it is made in all neurons when Cre recombinase is absent. Set difference strategy: when h56D-Cre and hSYN-$(EGFP_{FWD})^{Cre}$ viruses are co-injected, Cre recombinase shuts off EGFP expression in inhibitory but not in excitatory neurons.

(B) Brain sections were analyzed by *in situ* mRNA hybridization using probes to EGFP (green) and to endogenous glutamic acid decarboxylase (GAD65; red) transcripts. Mouse hippocampal area CA1 following subtraction: Cre-expressing GABAergic interneurons lacked EGFP (88.8% ± 1.0% $GAD65^+$ cells were $EGFP^-$, n = 3 sections, 2 mice, 61 $GAD65^+$ cells), while putative stratum pyramidale excitatory neurons continued to express EGFP. Cell nuclei were DAPI stained (blue) to confirm hippocampal layers. so, stratum oriens; sp, stratum pyramidale. Scale bars, 20 μm.

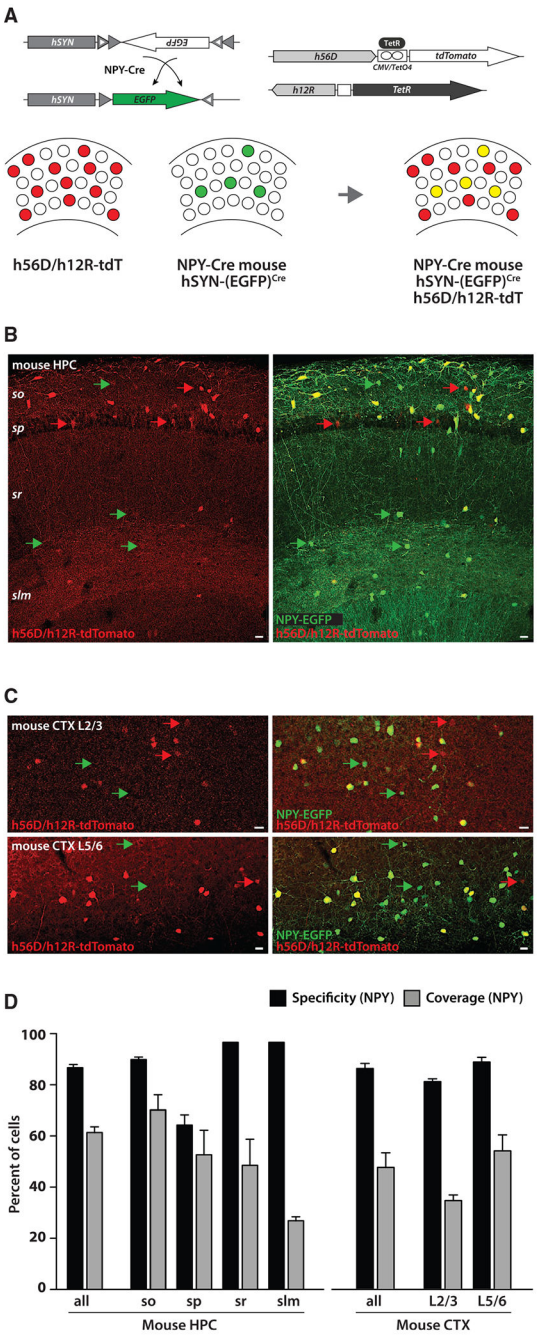

Figure 7. Set Difference Strategy to Target Mouse Hippocampal NPY$^+$ Interneurons

(A) A mix of three rAAVs shown in the schematic was injected into *NPY-Cre* mouse dorsal hippocampus and cortex (see Method Details in STAR Methods). hSYN-(EGFP)^{Cre} was used to label endogenous Cre-expressing neurons green. h56D$_{TetO4}$-tdTomato and h12R-TetR vector mix (h56D/h12R-tdTomato) was used to label virus-targeted neurons red. Double-labeled NPY$^+$/tdT$^+$ neurons are shown in yellow.

(B) Dorsal hippocampus: most virus-targeted neurons were NPY$^+$, but not all NPY$^+$ neurons were labeled (green arrows). Most of the labeled NPY$^-$ cells (red arrows) were VIP$^+$ (Figure

S7C). Virus-targeted NPY^+/tdT^+ neurons were primarily in stratum oriens. so, stratum oriens; sp, stratum pyramidale; sr, stratum radiatum; slm, stratum lacunosum-moleculare. Scale bars, 20 μm.

(C) Cortical layers 2/3 and 5/6 (no virus-targeted cells were observed in layer 4): as in (B), most virus-targeted neurons were NPY^+, but not all NPY^+ neurons had been labeled (green arrows). Red arrows mark NPY^-/tdT^+ neurons, which were not characterized. Scale bars, 20 μm.

(D) Virus-targeted NPY^+ neuron counts plotted as mean ± SE. Mouse HPC: specificity 89.7% ± 1.3%, coverage 63.5% ± 2.3%; so: specificity 93.1% ± 1.0%, coverage 72.6% ± 6.2%; sp: specificity 66.5% ± 4.0%, coverage 54.5% ± 9.9%; sr: specificity 100%, coverage 50.2% ± 10.5%; slm: specificity 100% ± 0%, coverage 27.8% ± 1.6% (n = 8 sections, 3 mice, 165 $EGFP^+$ cells). Mouse CTX: specificity 87.9% ± 1.8%, coverage 44.9% ± 3.5% (n = 4 sections, 2 mice, 305 $EGFP^+$ cells, >1,500 cells total); L2/3 specificity 83.4% ± 1.1%, coverage 35.4% ± 2.3% (n = 2 sections, 2 mice, 107 $EGFP^+$ cells); L5/6 specificity 91.4% ± 1.9%, coverage 55.6% ± 6.4%, (n = 4 sections, 2 mice, 166 $EGFP^+$ cells).

KEY RESOURCES TABLE

REAGENT or RESOURCE	SOURCE	IDENTIFIER
Antibodies		
Rabbit anti-PV	Swant	Cat#PV-25/28
Rat anti-SST	Millipore	Cat#MAB354
Alexa Fluor Secondary Antibodies	ThermoFisher	N/A
Bacterial and Virus Strains		
rAAV2/7:h12a-tdTomato	This Paper	N/A
rAAV2/7:h12RL-EGFP	This Paper	N/A
rAAV2/7:h12R-tdTomato	This Paper	N/A
rAAV2/7:h12D-EGFP	This Paper	N/A
rAAV2/7:h56D-tdTomato	This Paper	N/A
rAAV2/7:h56iiD-tdTomato	This Paper	N/A
rAAV2/7:h56iiR-tdTomato	This Paper	N/A
rAAV2/7:h56R-EGFP	This Paper	N/A
rAAV2/1:h56D-GCaMP6f	This Paper	N/A
rAAV2/7:h56D-$(EGFP)^{Cre}$	This Paper	N/A
rAAV2/1:h56D-$(EGFP)^{Cre}$	This Paper	N/A
rAAV2/1:h56D-$(EGFP)^{Flp}$	This Paper	N/A
rAAV2/1:hSYN-$(EGFP)^{Cre}$	This Paper	N/A
rAAV2/1:hSYN-Cre	This Paper	N/A
rAAV2/7:SST-EGFP	This Paper	N/A
rAAV2/7:SST-Cre	This Paper	N/A
rAAV2/1:SST-Flp	This Paper	N/A
rAAV2/7:PV-EGFP	This Paper	N/A
rAAV2/1:PaqR4-Cre	This Paper	N/A
rAAV2/1:PaqR4-EGFP	This Paper	N/A
rAAV2/1:hSYN-$(EGFP_{FWD})^{Cre}$	This Paper	N/A
rAAV2/1:CamKII-Cre	This Paper	N/A
rAAV2/7:h56D-Cre	This Paper	N/A
rAAV2/7:h12R-TetR	This Paper	N/A
Chemicals, Peptides, and Recombinant Proteins		
Isoflurane	Patterson Veterinary	Cat# 14043-704-06
DMEM	GIBCO-BRL	Cat#11995-065
Fetal Bovine Serum	GIBCO-BRL	Cat#10437010
Penicillin-Streptomycin	GIBCO-BRL	Cat#15140122
OCT	TissueTek	Cat#4583
DAPI Fluoromount-G	Southern Biotech	Cat#0100-20
Metabond	Parkell	Cat#S396

REAGENT or RESOURCE	SOURCE	IDENTIFIER
Normal Goat Serum	ThermoFisher	Cat#50062Z
Normal Donkey Serum	ThermoFisher	Cat#NC9719162
jetPEI	PolyPlus	Cat#101
Critical Commercial Assays		
RNAscope Flourescent Multiplex Reagents	Advanced Cell Diagnostics	Cat#320850
Experimental Models: Cell Lines		
HEK293T	ATCC	CRL-11268
Experimental Models: Organisms/Strains		
Mouse: C57BL/6J mouse	Jackson Laboratory	Cat#000664
Mouse: 129S1/SvlmJ	Jackson Laboratory	Cat#002448
Mouse: *B6.Cg-Npy$^{tm1(cre)Zman}$*/J	Jackson Laboratory	Cat#027851
Mouse: *B6.Cg-Gt(ROSA)26Sor$^{tm14(CAG-tdTomato)Hze}$*/J	Jackson Laboratory	Cat#007914
Mouse: PV-Cre	Scholl et al., 2015	N/A
Mongolian gerbil: Crl:MON(Tum)	Charles River	Cat#243
Primate: Marmoset	TxBiomed	N/A
Primate: Rhesus macaque	Covance SA TX	N/A
Primate: Rhesus macaque	University of Louisiana	N/A
Recombinant DNA		
hSYN$_{TetO4}$-tdTomato	This Paper	N/A
CAG-TetR	This Paper	N/A
Software and Algorithms		
ImageJ	https://fiji.sc/	N/A
Maestro software suite	https://sites.google.com/a/srscicomp.com/maestro/	N/A
SArKS	Wylie et al., 2018	N/A
ECR browser	Ovcharenko et al., 2004	N/A
Kallisto	Bray et al., 2016	N/A
SIMA software suite	Kaifosh et al., 2014	N/A
Other		
RNAscope Mm Pvalb probe	Advanced Cell Diagnostics	Cat#421931
RNAscope Mm SST probe	Advanced Cell Diagnostics	Cat#404631
RNAscope Mm NPY probe	Advanced Cell Diagnostics	Cat#313321
RNAscope Mm GAD2 probe	Advanced Cell Diagnostics	Cat#439371
RNAscope EGFP probe	Advanced Cell Diagnostics	Cat#400281
RNAscope tdTomato probe	Advanced Cell Diagnostics	Cat#317041